Genetic risk for Multiple Sclerosis originated in Pastoralist Steppe populations

Authors
William Barrie[1]§, Yaoling Yang[2,3]§, Kathrine E. Attfield[4]§, Evan Irving-Pease[5]§, Gabriele Scorrano[5]§, Lise Torp Jensen[6]§, Angelos P. Armen[4], Evangelos Antonios Dimopoulos[7], Aaron Stern[8], Alba Refoyo-Martinez[5], Abigail Ramsøe[5], Charleen Gaunitz[5], Fabrice Demeter[5], Marie Louise S. Jørkov[9], Stig Bermann Møller[10], Bente Springborg[10], Lutz Klassen[11], Inger Marie Hyldgård[11], Niels Wickmann[12], Lasse Vinner[5], Thorfinn Sand Korneliussen[5], Martin Sikora[5], Kristian Kristiansen[5,13], Santiago Rodriguez[3], Rasmus Nielsen[5,8], Astrid K. N. Iversen[4]@, Daniel J. Lawson[2,3]*@, Lars Fugger[4,14]*@, Eske Willerslev[1,5]*@

Affiliations
[1]Department of Zoology, University of Cambridge, Cambridge, UK,
[2]Department of Statistical Sciences, School of Mathematics, University of Bristol, Bristol, UK,
[3]Integrative Epidemiology Unit, Population Health Sciences, University of Bristol, Bristol, UK,
[4]Oxford Centre for Neuroinflammation, Nuffield Department of Clinical Neurosciences, John Radcliffe Hospital, University of Oxford, Oxford, UK
[5]Lundbeck Foundation GeoGenetics Centre, Globe Institute, University of Copenhagen, Copenhagen, Denmark,
[6]Department of Clinical Medicine, Aarhus University Hospital, Aarhus, Denmark
[7]Pathogen Genomics and Evolution Group, Department of Veterinary Medicine, University of Cambridge, Cambridge, UK
[8]Department of Integrative Biology, University of California, Berkeley
[9]Laboratory of Biological Anthropology, Department of Forensic Medicine, University of Copenhagen, Denmark
[10]Ålborg Historiske Museum, Nordjyske Museer, Vang Mark 25, 9380 Vestbjerg, Denmark
[11]Museum Østdanmark - Djursland og Randers. Stemannsgade 2, DK-8900 Randers C, Denmark
[12]Museum Vestsjælland, Forten 10, 4300 Holbæk, Denmark
[13]Department of Historical Studies, University of Gothenburg, SE-41255, Gothenburg, Sweden
[14]MRC Human Immunology Unit, John Radcliffe Hospital, University of Oxford, Oxford, UK

* Corresponding authors; email: Dan.Lawson@bristol.ac.uk, lars.fugger@ndcn.ox.ac.uk, ew482@cam.ac.uk
§ Joint first authors
@ Joint last authors

SUMMARY
Multiple sclerosis (MS) is a modern neuro-inflammatory and -degenerative disease, which is most prevalent in Northern Europe. Whilst it is known that inherited risk to MS is located within or within close proximity to immune genes it is unknown when, where and how this genetic risk originated. By using the largest ancient genome dataset from the Stone Age, along with new Medieval and post-

Medieval genomes, we show that many of the genetic risk variants for MS rose to higher frequency among pastoralists located on the Pontic Steppe, and were brought into Europe by the Yamnaya-related migration approximately 5,000 years ago. We further show that these MS-associated immunogenetic variants underwent positive selection both within the Steppe population, and later in Europe, likely driven by pathogenic challenges coinciding with dietary and lifestyle environmental changes. This study highlights the critical importance of this period as a determinant of modern immune responses and its subsequent impact on the risk of developing MS in a changing environment.

INTRODUCTION

Multiple sclerosis (MS) is an autoimmune disease of the brain and spinal cord that currently affects more than 2.5 million people worldwide. The prevalence varies markedly with ethnicity and geographical location, with the highest prevalence observed in Europe (142.81 per 100.000 people), and Northern Europeans being particularly susceptible to developing the disease[1]. The origins and reasons for the geographical variation are poorly understood, yet such biases may hold important clues as to why the prevalence of autoimmune diseases, including MS, has continued to rise during the last 50 years.

While still elusive, MS etiology is thought to involve gene-gene and gene-environmental interactions. Accumulating evidence suggests that exogenous triggers initiate a cascade of events involving a multitude of cells and immune pathways in genetically vulnerable individuals, which may ultimately lead to MS neuropathology[2].

Genome-wide association studies have identified 233 commonly occurring genetic variants that are associated with MS; 32 variants are located in the HLA region and 201 outside the HLA region[3]. The strongest MS associations are found in the HLA region with the most prominent of these, HLA-DRB1*15:01, conferring an approximately three-fold increase in the risk of MS. Collectively, genetic factors are estimated to explain approximately 30% of the overall disease risk, while environmental and lifestyle factors are considered the major contributors to MS. Such determinants may include geographically varying exposures like infections and low sun exposure/vitamin D deficiency. For instance, while infection with Epstein-Barr virus frequently occurs in childhood and usually is symptomless, delayed infection into early adulthood, as typically observed in countries with high standards of hygiene, is associated with a 32-fold increased risk of MS[4,5]. Lifestyle factors associated with increased MS risk such as smoking, obesity during adolescence, and nutrition/gut health also vary geographically[6]. Dysregulations including autoimmunity in modern immune systems could also result from the absence of ancient immunological triggers to which humans have evolutionarily adapted, for instance by disturbing the delicate balance of pro- and anti-inflammatory pathways[7].

European ancestry has been postulated to explain part of the global difference in MS prevalence globally in admixed populations[8]. Specifically, cases in African Americans exhibit increased European ancestry in the HLA region compared to controls, with European haplotypes conferring more MS risk for most HLA alleles, including HLA-DRB1*15:01. Conversely, Asian American cases have decreased European ancestry in the HLA region compared to controls. Although Ancient European ancestry and MS risk in Europe are known to be geographically structured (Figure 1a-b), the effect of ancestry variation within Europe on MS prevalence is unknown.

Modern ancestry is viewed as a mixture of genetic ancestries derived from ancient populations, who can be distinguished by their subsistence lifestyle: Western Hunter-Gatherers (WHG), Eastern

Hunter-Gatherers (EHG), Caucasus Hunter-Gatherers (CHG), Anatolian Farmers, and Steppe Pastoralists (Figure 1c-d). Using the largest ancient genome dataset from the Stone Age, presented in the accompanying study 'Population Genomics of Stone Age Eurasia'[9], coupled with new Medieval and post-Medieval genomes, we quantified modern European ancestry with respect to these ancient ancestries to identify signals of lifestyle-specific evolution. Then we determined whether the variants associated with an increased risk for MS have undergone positive selection. We asked when selection occurred and whether the targets of selection were specific to diet and lifestyle. Finally, we examined the environmental conditions that may have caused selection for risk variants, including human subsistence practice and exposure to pathogens.

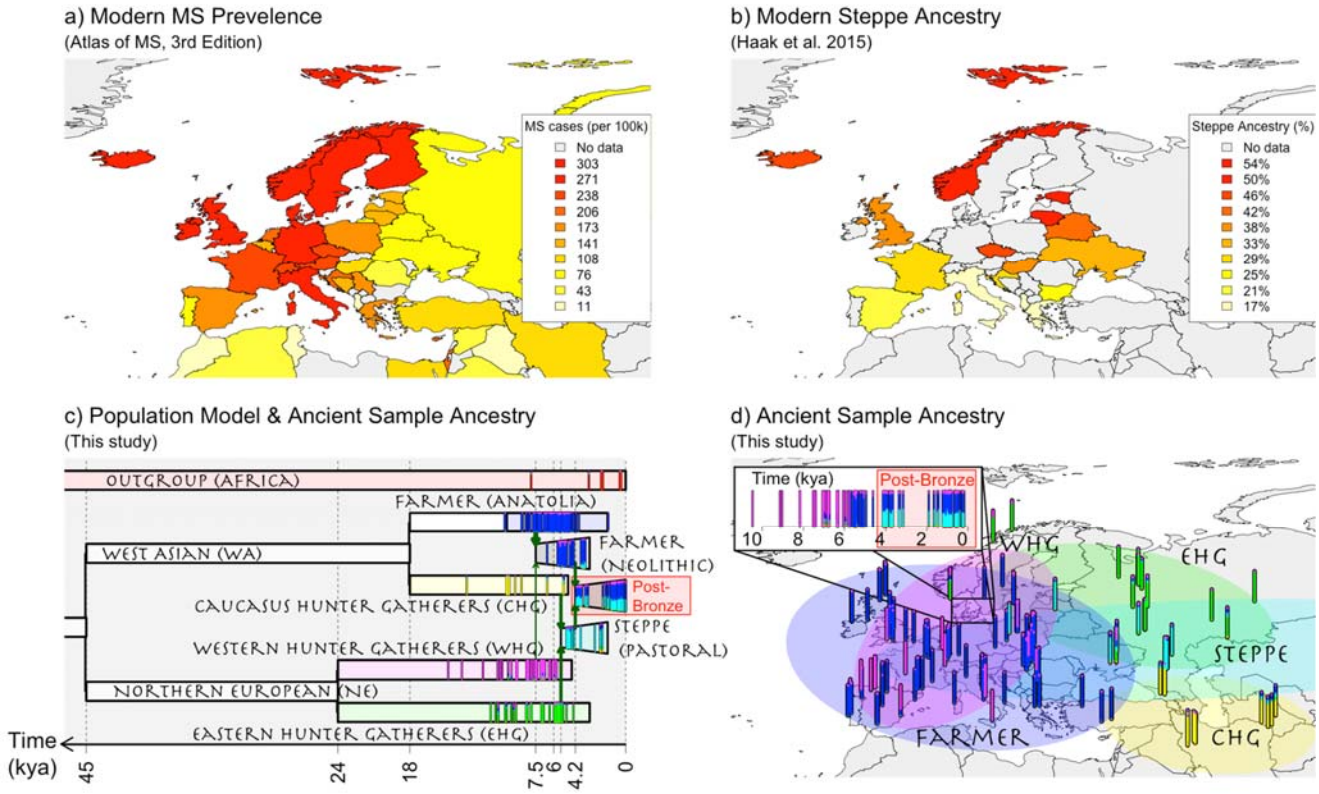

Figure 1: Population history of Europe is associated with modern-day distribution of MS. *a) Modern-day geographical distribution of MS in Europe. Prevalence data for MS (cases per 100,000) was obtained from [1]. b) Steppe ancestry in modern samples as estimated by [10]. c-d) A model of European prehistory[11] onto which our reference samples have been projected using NNLS (see Methods), and the same data represented spatially. Chronologically, Western Hunter-Gatherers (WHG) and Eastern Hunter-Gatherers (EHG) were largely replaced by Anatolian Farmers amid demographic changes during the "Neolithic transition" around 9,000 years ago. Later migrations during the Bronze Age about 5,000 years ago brought a roughly equal Steppe ancestry component from the Pontic-Caspian Steppe to Europe, an ancestry descended from the EHG from the Middle Don River region and Caucasus Hunter-Gatherers (CHG)[9]. Steppe ancestry has been associated with the Yamnaya culture and then with the expansion westwards of the Corded Ware Complex and Bell Beaker culture, and the eastwards expansion in the form of the Afanasievo culture[12,10]. Samples are vertical bars representing their "admixture estimate" estimated by NNLS (methods) from six*

ancestries: EHG (green), WHG (pink), CHG (yellow), Farmer (blue), Steppe (cyan) or an Outgroup (represented by ancient Africans, red). Important population expansions are shown as growing bars and "recent" (post-Bronze age) non-reference admixed populations are shown for the Denmark time-transect (see Supplementary Figure 1.1 for details).

RESULTS

We obtained local ancestry (i.e. ancestry at specific loci) labels for ~410,000 self-identified "white British" individuals in the UK Biobank[13], using a reference panel of 318 ancient DNA (aDNA) samples[9] (Figure 1; Supplementary Figure 1.1) from the Mesolithic and Neolithic, including Steppe pastoralists. Comparing the ancestry at each labelled single nucleotide polymorphism (SNP, n=549,323) to genome-wide ancestry in the UK Biobank provided a "local ancestry anomaly score" (Methods), for which two regions stood out as having undergone the most significant ancestry-specific evolution in this period: LCT/MCM6, regulating lactase persistence[14], and the HLA region (Figure 2, top).

To determine whether this evolution of the HLA region has subsequently impacted diseases that are strongly associated with risk alleles found within this region, we investigated the history of variants associated with two HLA-associated autoimmune diseases, multiple sclerosis (MS) and rheumatoid arthritis (RA), using the largest ancient genome dataset from the Stone Age coupled with 86 new Medieval and post-Medieval genomes from Denmark (Supplementary Figure 1.1, Supplementary Note 1, ST1). Alongside modern data, with our newly published genomes we have an almost complete transect from approximately 10,000 years ago to the present.

The allele frequencies of SNPs conferring the highest risk for MS (all in the HLA class II region) in our ancient groups show striking patterns. In particular the tag SNP (rs3135388-T) for HLA-DRB1*15:01, the largest risk factor for MS, first appeared in an Italian Neolithic individual (sampleId R3 from Grotta Continenza, C14 dated to between 5,836-5,723 BCE, coverage 4.05X) and rapidly increased in frequency around the time of the emergence of the Yamnaya culture around 5,300 years ago in Steppe and Steppe-derived populations (Figure 2). From risk allele frequencies of individuals in the UK Biobank born in, and of a 'typical ancestral background' for, each country[9], we found HLA-DRB1*15:01 frequency peaks in modern populations of Finland, Sweden and Iceland, and in ancient populations with high Steppe ancestry (Figure 2, inset).

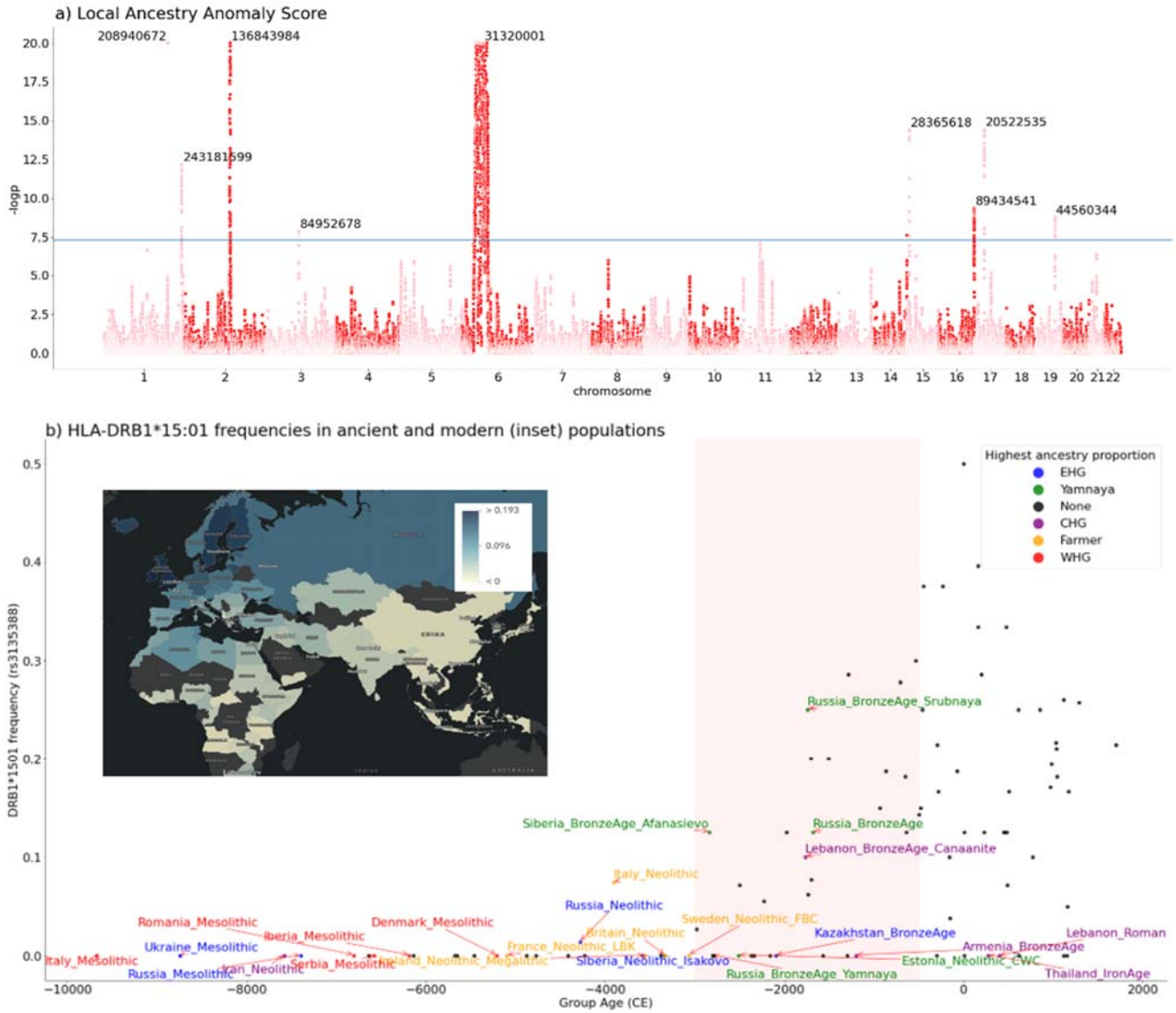

Figure 2. Areas of unusual local ancestry in the genome, and ancient and modern frequencies of DRB1*15:01.

*a): Local Ancestry Anomaly Score measuring the difference between the local ancestry and the genome-wide average (capped at -log10(p)=20; see Methods). b) HLA-DRB1*15:01 frequencies in ancient and modern (inset) populations; this is the highest effect variant for MS risk (calculated using rs3135388 tag SNP). For the ancient data, for each ancestry (CHG, EHG, WHG, Farmer, Steppe) the five populations with the highest amount of that ancestry are coloured and labelled. DRB1*15:01 was present before the Steppe expansion, but rose to high frequency during the Yamnaya formation (shaded red). The geographical distribution of DRB1*15:01 frequency in modern populations in the UK Biobank is also shown (inset).*

To investigate the risk of a particular ancestry at all MS-associated fine-mapped loci[3] present in the UK Biobank imputed dataset (n=205/233, see methods), we used the local ancestry dataset to calculate a risk ratio (see Methods: Weighted Average Prevalence) for each ancestry. For MS, Steppe ancestry has the highest risk ratio in nearly all HLA SNPs, while Farmer and 'Outgroup' ancestry (represented by ancient Africans) are often the most protective (Figure 3, top), meaning a Steppe-derived haplotype at these positions confers MS risk.

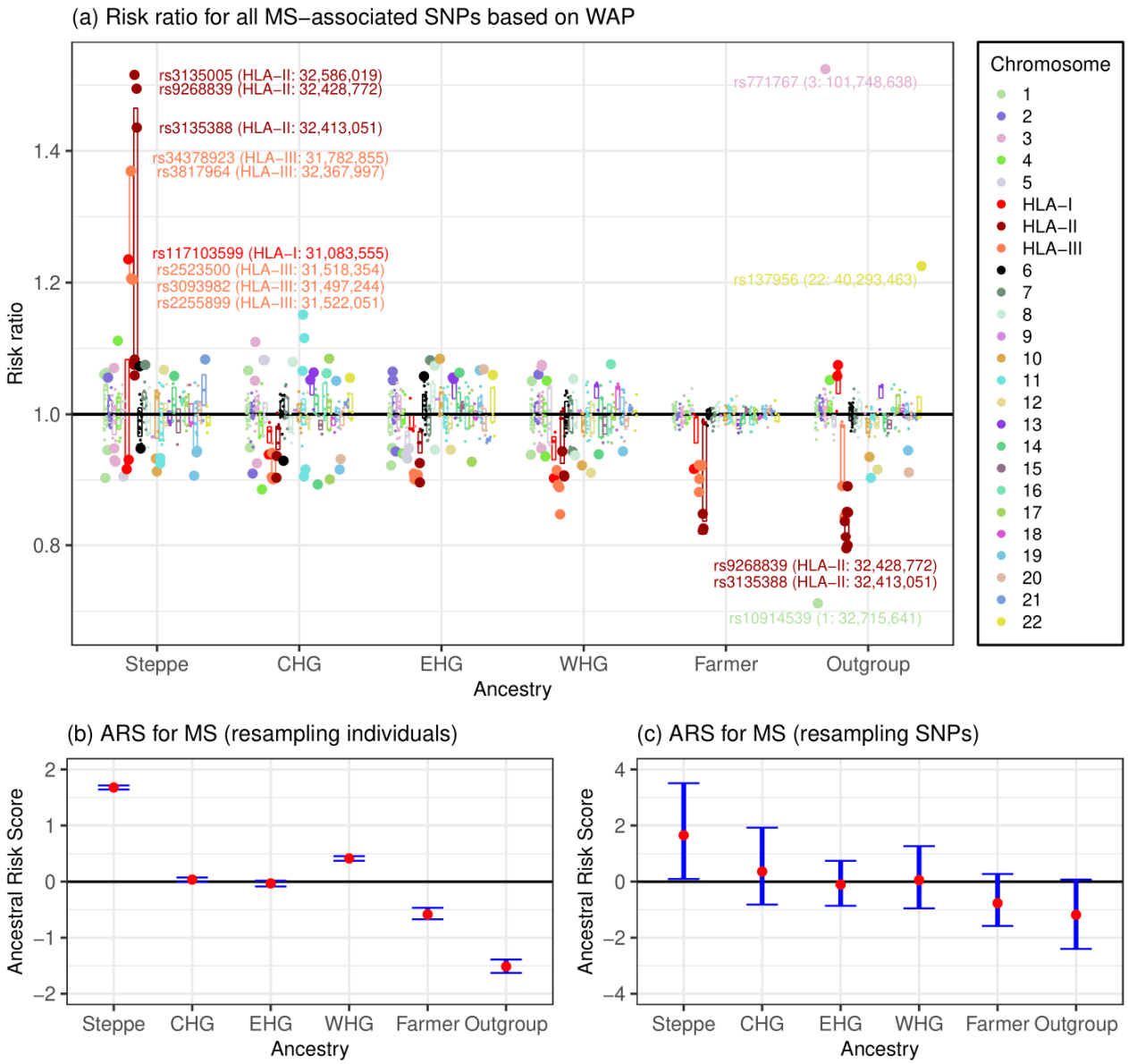

Figure 3: Associations between local ancestry and MS in a modern population.
a) Risk ratio of SNPs for MS based on weighted average prevalence (WAP; see Methods), when decomposed by inferred ancestry. Each ancestry is assigned a mean and confidence interval based on bootstrap resampling, for each chromosome (faded where non-significant). The three HLA regions are split from the rest of chromosome 6, and SNPs with risk ratio >1.2 or <0.8 are annotated. b-c) Genome-wide Ancestral Risk Scores (ARS, see Methods) for MS. Confidence intervals are estimated by either bootstrapping over individuals (b, which can be interpreted as testing power to reject a null of no association between MS and ancestry) and bootstrapping over SNPs (c, which can be interpreted as testing whether ancestry is associated with MS genome-wide).

Having shown that some ancestries carry higher risk, we calculated an aggregate risk for each ancestry across the same SNPs using a new statistic, the Ancestral Risk Score (ARS). ARS is computed in a large modern sample with local ancestry labels, estimating the relative risk for a

186 modern individual consisting of entirely one ancestry, mitigating the effects of low aDNA sample
187 numbers and bias[15], and being robust to intervening drift and selection. We used effect size estimates
188 from previous association studies, under an additive model, with confidence intervals obtained via an
189 accelerated bootstrap[16] (Supplementary Note 4). In the ARS for MS (Figure 3 bottom), Steppe
190 ancestry had a large and significant risk, followed by WHG, CHG and EHG; Neolithic Farmer and
191 Outgroup ancestry had the lowest ARS (Figure 3). Therefore Steppe ancestry is contributing the most
192 risk for MS overall. We tested for a genome-wide association by resampling loci, and found that
193 Steppe risk is much reduced but still clearly exceeds Farmer, a pattern which holds even when
194 excluding SNPs on the HLA (Supplementary Note 4, Figure S4.1).
195
196 The fact that all but two MS-associated HLA SNPs confer risk within Steppe ancestry implies that
197 this risk has a common evolutionary history. We therefore investigated whether ancestry was
198 important for prediction using three types of association study in the UK Biobank for disease-
199 associated SNPs, controlling for age, sex and the first 18 PCs. The first of these is a regular SNP-
200 based association as conducted in GWAS. The second uses local ancestry probabilities instead of
201 genotype values (Supplementary Note 3). The third is based on Haplotype trend regression (HTR)
202 which is used to detect interactions between SNPs[17] by treating each haplotype's probability as a
203 feature from which to predict a trait, instead of using SNPs as in a regular GWAS. We developed a
204 new method called Haplotype Trend Regression with eXtra flexibility (HTRX, Supplementary Note
205 5) that searches for haplotype patterns that include single SNPs and non-contiguous haplotypes. To
206 prevent overfitting, we reported out-of-sample variation explained, and showed by simulation (see
207 Supplementary Figure 4.4) that HTRX predicts the same variance as regular GWAS when interactions
208 are absent, but explains more variance when the interaction strength increases.
209
210 Although our cohort of self-identified "white British" individuals is relatively under-powered with
211 respect to MS (cases=1,949; controls=398,049; prevalence=0.487%), MS was associated with Steppe
212 and Farmer ancestry ($p<1e-10$) in the HLA region (Supplementary Figure 4.1). In 3 out of 4 main LD
213 blocks within the HLA (class I, two subregions of class II determined by LD blocks at 32.41-32.68Mb
214 and 33.04-33.08Mb, and class III), local ancestry explains significantly more variation in total than
215 SNP variation (Figure 4; measured by average out-of-sample McFadden's R^2 for logistic regression,
216 see Methods). While increased ancestry performance over GWAS can be explained by tagging of
217 SNPs outside the region, increased HTRX performance over GWAS quantifies the total effect of a
218 haplotype, including rare SNPs and epistasis. Across the entire HLA region, haplotypes explain at
219 least 17% more out-of-sample variation than GWAS (2.90%, compared to 2.48%). Interaction signals
220 are also observed within class I, within class II, and between class I and III.
221

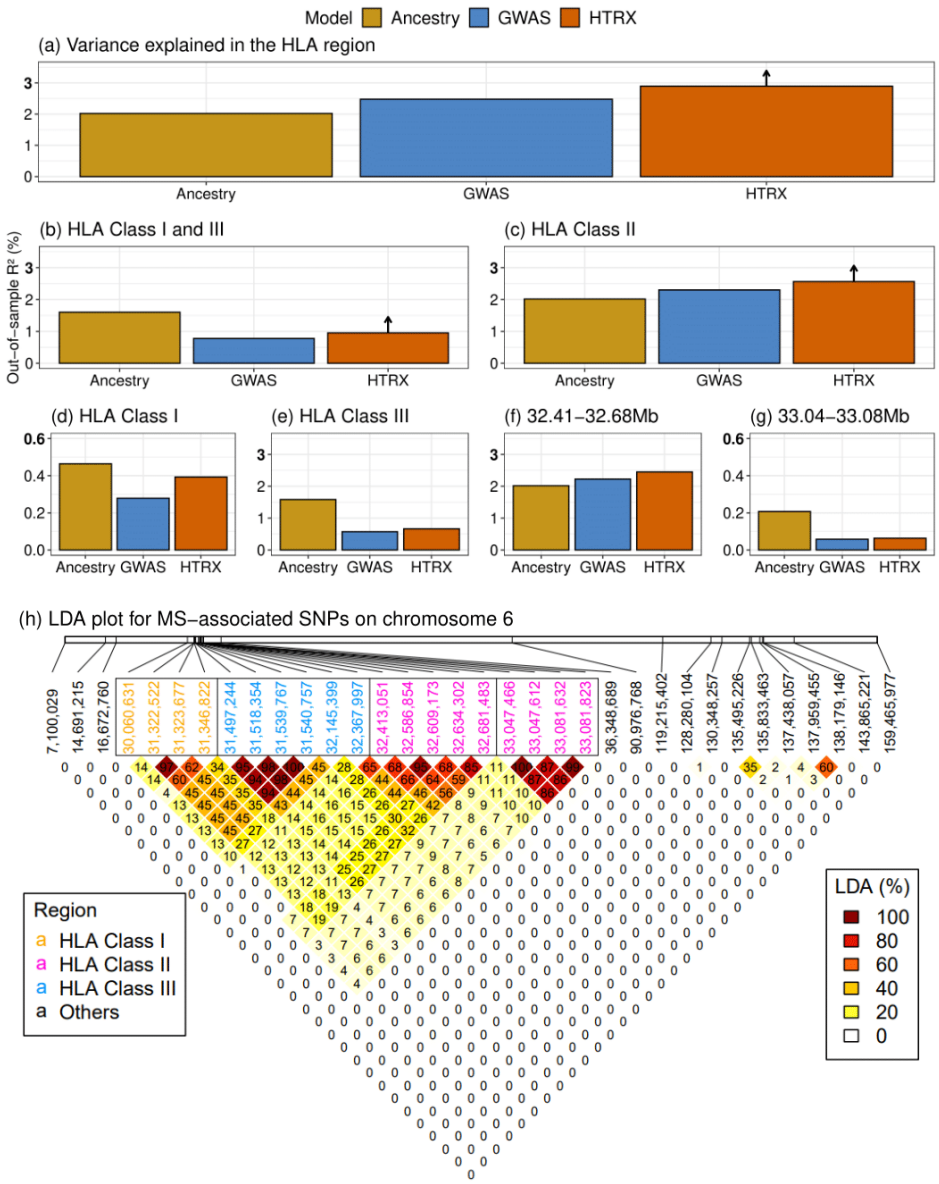

Figure 4: MS association in the HLA.

Comparison of variance explained in MS within the UK Biobank, for all fine-mapped HLA SNPs with an independent contribution[3]*. The plots compare GWAS (treating SNPs as having independent effect), local ancestry at those SNPs, and HTRX (haplotypes) after accounting for covariates (Methods). a) is for fine-mapped MS-associated SNPs in the HLA. b) is HLA class I and -III, c) is HLA class II, d) is HLA class I, e) is HLA class III, f) and g) are subregions of HLA class II chosen from LD. HTRX has small "up-arrows" where these are lower bounds (Methods). h) Genetic correlations in the HLA region at our time-depth from Ancestry-based LD (LDA, see Methods) and Supplementary Figure 6.5 for LD.*

This interaction risk can be attributed to particular ancestries: for example, multiple haplotypes at the 32.41-32.68Mb region are Steppe-associated and have high MS odds ratios. We further tested whether co-occurring ancestries at each loci were associated with MS (Methods; Supplementary Figure 4.2), but found no evidence that risk was associated with anything other than Steppe ancestry.

Having established that Steppe ancestry contributes most of the HLA-associated risk for MS, we investigated evidence for polygenic selection on the disease-associated variants using two methods. Firstly, we used a novel chromosome painting technique based on inference of a sample's nearest neighbours in the marginal trees of an ARG that contains labelled individuals (Irving-Pease et al., *submitted*). The resulting ancestral path labels, for haplotypes in both ancient and modern individuals, allowed us to infer allele frequency trajectories for risk associated variants, while controlling for changes in admixture proportions through time. These paths extend backwards from the present day to approximately 15,000 years ago, and are labelled with the unique population that a path travels through. We stress that the path labels are not representative of a continuous population, but represent a path backwards in time that encompasses that ancestry. For example, the CHG path originates in Caucasus hunter-gatherers, before merging with EHG to form the Steppe population, and then merges with other ancestries in later European populations (Figure 1).

Because not all fine-mapped SNPs had ancestral path labels (missing OR=10.4%) and due to the difficulty in accurately inferring HLA alleles in ancient samples[18], we LD-pruned genome-wide significant summary statistics from the same study[3] for which we did have ancestry path labels (n=62, see methods). This allowed us to test for polygenic selection across disease-associated variants using CLUES[19] and PALM[20].

For MS, we found evidence that disease risk was selectively increased when considering all ancestries collectively (p=5.06e-05; ω=0.0029), between 5,000-2,000 years ago (Figure 5). Conditioning on each of the four long-term ancestral paths (CHG, EHG, WHG and ANA), we found a statistically significant signal of selection in CHG (p=6.45e-3; ω=0.009). None of the other ancestral paths reached nominal significance, although ANA (p=0.0743; ω=0.011) and EHG (p=0.064; ω=0.0045) paths were close. Again, it is likely that the selection occurred in the pastoralist population of the Steppe, as that population consists of approximately half CHG ancestry[11] (Figure 1). The SNP driving the largest change in genetic risk over time was rs3129934, in both the pan-ancestry (p=9.52e-06; s=0.017) and CHG (p=0.019; s=0.008) analyses, which tags the HLA-DRB1*15:01 haplotype[21]. We also tested three other alleles that tag the HLA-DRB1*15:01 haplotype (rs3129889, rs3135388 and rs3135391) for evidence of selection, and found that the ancestry stratified signal was consistently strongest in CHG (Figure 5). None of the four tag SNPs were detected on either the EHG or WHG backgrounds, indicating that the HLA-DRB1*15:01 haplotype likely originated in the basal population ancestral to both ANA and CHG.

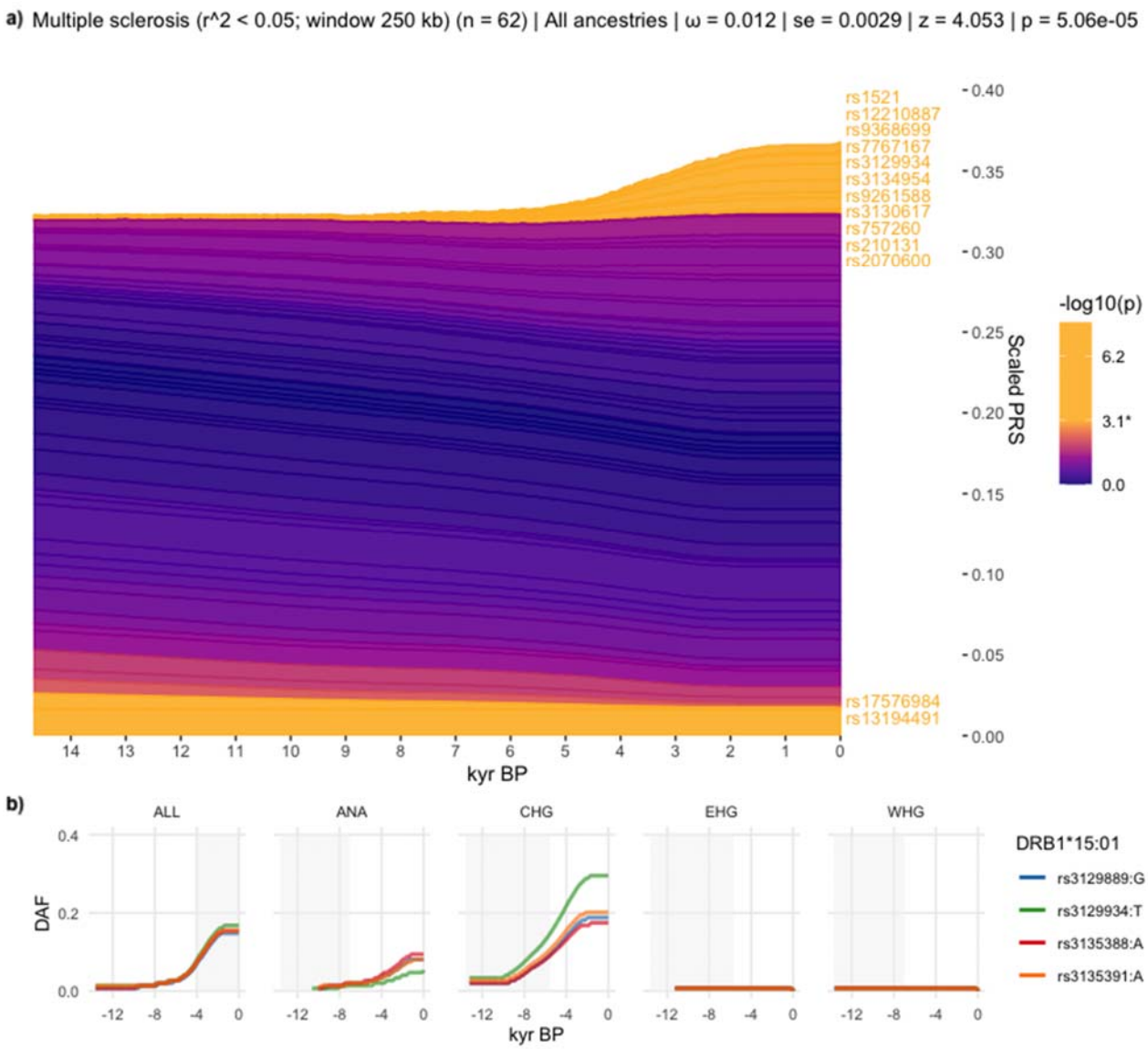

Figure 5: Evidence for selection on MS-associated SNPs.
a) Stacked line plot of the pan-ancestry PALM analysis for MS, showing the contribution of alleles to disease risk over time. Individual SNPs are stacked, with their trajectories polarised to show the frequency of the positive risk allele and weighted by their scaled effect size: when a given SNP bar becomes wider over time the risk allele has increased in frequency, and vice versa. SNPs are sorted by their marginal p-value and direction of effect, with selected SNPs that increase risk plotted on top. SNPs are also coloured by their marginal p-values, and significant SNPs are shown in yellow. The y-axis shows the scaled polygenic risk score (PRS), which ranges from 0 to 1, representing the maximum possible additive genetic risk in a population.
*b) Maximum likelihood trajectories for four SNPs tagging DRB1*15:01. The background is shaded for the approximate time period in which the ancestry existed as an actual population. None of the tagging alleles are present on the EHG or WHG ancestral paths.*

Our second selection measure introduces a new statistic, Linkage Disequilibrium of Ancestry (LDA). LDA is the correlation between ancestries across SNPs, measuring whether recombination events between ancestries are high compared to recombination within ancestries. From this we constructed

289 an “LDA score” using the fine-mapped SNPs, which is the total amount of genome in LDA with a
290 given SNP. A high LDA score indicates that the haplotype inherited from the reference population is
291 longer than expected, while a low score indicates that the haplotype is shorter than expected (i.e.
292 underwent more recombination). For example, the LCT/MCM6 region exhibits a high LDA score
293 (Supplementary Figure 6.4), as expected from a relatively recent selective sweep[22].
294
295 The HLA has significantly *lower* LDA scores than the rest of chromosome 6 (Supplementary Figure
296 6.4). We simulated the LDA score under selection (Supplementary Figure 6.1; Methods), which
297 showed that when SNP frequencies are increasing in the most recent population, single locus selection
298 cannot explain this signal (Supplementary Figure 6.2-3). Instead, different loci in LD must have
299 independently reached high frequency in different ancestral populations that admixed, with selection
300 favouring haplotypes of mixed ancestry over single-ancestry haplotypes. Although multi-SNP
301 selection has been modelled[23], the interaction with prior population structure is less explored and is
302 important for the HLA, justifying a new term, "recombinant favouring selection".
303
304 The HLA region contains the highest “Outgroup” ancestry anywhere on the genome (Figure 6),
305 reflecting high nucleotide diversity. Unlike other measures of balancing selection such as Fst (Figure
306 6), LDA describes excess ancestry LD from specific, dated populations and therefore need not be
307 correlated with them. For the HLA class II region, the selection measures all line up (LDA score, Fst,
308 pi), but for class I, the LDA score has an additional non-diverse minimum at 30.8Mb, implying that
309 here the genome is ancestrally diverse but genetically strongly constrained. The LDA score is thus
310 informative about the type of selection being detected, and whether it has been subject to change.
311

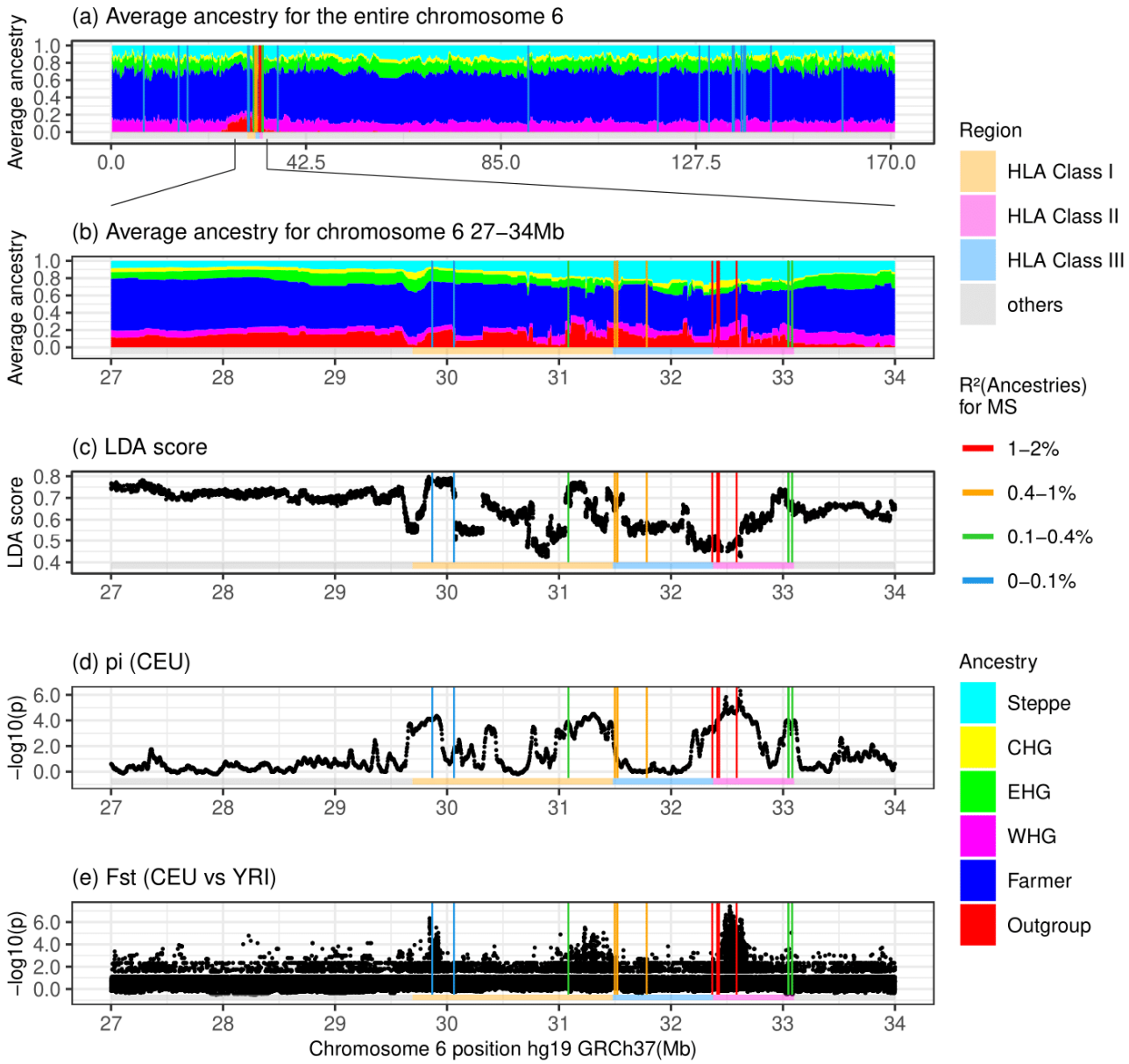

Figure 6: Signatures of selection at the HLA locus showing different regions of the HLA (coloured bar) and locations of MS-associated SNPs (vertical lines, coloured by the variance explained by 6 ancestries). *a): Whole Chromosome 6 "local ancestry" decomposition by genetic position. b). HLA "local ancestry" decomposition. c): LDA score; low values are indicative of selection for multiple linked loci, while high values indicate positive selection. d): pi scores (nucleotide diversity) for CEU (Northern and Western European ancestry). MS-associated SNPs fall in highly diverse regions of the HLA. e): Fst scores (divergence between two populations) for CEU vs YRI(Yoruba); locally higher scores indicate regions that have undergone differential selection between the two populations.*

Because MS would not have conferred a fitness advantage on ancient individuals, it is likely that this selection was driven by traits with shared genetic architecture, of which increased risk for MS in the present is a consequence. We therefore looked at LD-pruned MS-associated SNPs that showed statistically significant evidence for selection using CLUES (n=26) and which also had a genome-

327 wide significant trait association (p < 5e-8) in any of the 4,359 traits from the UK Biobank[13] (UK
328 Biobank Neale Lab, Round 2: http://www.nealelab.is/uk-biobank/). We found that many selected
329 SNPs are also associated with celiac disease (n=15), white blood cell/neutrophil count (n=15/n=15),
330 hypothyroidism (n=14) and haemoglobin concentration (n=14) (Supplementary Figure 7.1). This
331 raised the possibility that the selection had increased risk for both MS and celiac disease, and when
332 we tested celiac disease for polygenic selection, we found significant evidence for positive selection,
333 increasing genetic risk (p=9.65e-3; ω=0.846, Supplementary Note 6).
334
335 Because the UK Biobank is underpowered with respect to many traits and diseases, we also undertook
336 a manual literature search (see methods) for all SNPs that reached genome-wide significance for
337 association with MS in the summary stats (i.e., not LD-pruned, as independence is not required) and
338 which showed statistically significant evidence for selection using CLUES (n=94). We found that
339 most of the alleles under positive selection are associated with protective effects against specific
340 pathogens (virus, bacteria, fungi and parasites) and/or infectious diseases within one or several
341 ancestral paths (disease or pathogen associated/total selected in ancestry path: pan-ancestry 36/44;
342 ANA 24/31; CHG 25/29; EHG 27/35; WHG 9/10, Supplementary Note 8, ST13, Supplementary
343 Figure 8.1), although we note that GWAS data for many infectious diseases are not available. We
344 observed that the selected alleles had protective associations with several chronic viruses (EBV, VZV,
345 HSV, and CMV) and to viruses or diseases not associated with transmission in small hunter-gatherer
346 groups (e.g., measles, mumps, influenza, whooping cough). Moreover, many selected alleles
347 conferred a reduction of risk of parasites, of skin and subcutaneous tissue, gastrointestinal, respiratory,
348 urinary tract, and sexually transmitted infections, or of pathogens associated with these or other
349 infections (e.g., malaria, toxoplasmosis, entamoeba histolytica, clostridium difficile, tuberculosis,
350 streptococcus pyrogenes, and chlamydia) (Supplementary Note 8, ST13, Supplementary Figure 8.1).
351
352 We contrasted these findings for MS with results for RA, a common inflammatory HLA class II-
353 associated disease that primarily affects the joints causing pain, swelling and stiffness[24], which shows
354 a strikingly different ancestry risk profile. HLA-DRB1*04:01 is the largest genetic risk factor for RA;
355 in the CLUES analysis, the tag SNP for this allele (rs660895) displayed evidence of continuous
356 negative selection until approximately 3,000 years ago (p=4.63e-4, Supplementary Figure 5.1). We
357 found that WHG and EHG ancestries often confer the most risk at SNPs associated with RA (Relative
358 Risk ratio of RA-associated SNPs based on WAP, see Methods); and these ancestries have
359 contributed the greatest risk for RA on aggregate, reflected in a higher ARS for these ancestries
360 (Supplementary Note 4), while Steppe and Outgroup ancestry have the lowest scores (Supplementary
361 Figure 3.1). These results were recapitulated in the local ancestry GWAS (Supplementary Note 3).
362
363 We found that RA-associated SNPs have undergone negative polygenic selection (p=7.93e-3,
364 Supplementary Figure 5.1) over the last approximately 15,000 years; when this is decomposed by
365 ancestry path, we found significant evidence for negative selection in both the CHG (p=3.09e-5) and
366 ANA (p=1.20e-3) ancestry paths. We found no evidence for negative selection in the EHG and WHG
367 paths, although both show a trend of increasing risk, and EHG nears significance (p=0.0842).
368
369 These results demonstrate that genetic risk for RA was higher in the distant past, in contrast to MS,
370 with RA-associated risk variants present at higher frequencies in European hunter-gatherer
371 populations before the arrival of agriculture. In order to understand what caused the high risk in
372 hunter-gatherer populations and subsequent negative selection, we again undertook a manual
373 literature search for pleiotropic effects of SNPs associated with RA. Because the number of SNPs that
374 reached genome-wide significance in the GWAS study and also showed statistically significant

evidence for directional selection was large, we only analysed LD-pruned SNPs (n=42). We found that the majority of selected SNPs were associated with protection against distinct pathogens and/or infectious diseases across all paths (disease or pathogen associated/total selected in ancestry path: pan-ancestry 9/13; ANA 10/13; CHG 8/11; EHG 10/16; WHG 10/12). We found that selected RA-risk alleles were often linked to the same pathogens or diseases as in the MS analysis, although the number of protective associations to distinct pathogens were fewer (Supplementary Note 8, ST14, Supplementary Figure 8.1).

DISCUSSION

The last 10,000 years have seen some of the most extreme global experiments in lifestyle with the emergence of farming in some regions and a pastoral lifestyle in others. While 5,000 years ago farmer ancestry predominated across Europe, a relatively diverged ancestry arrived with the Steppe migrations around this time. We have shown that this ancestry contributes the most genetic risk for MS today, and that these variants were the result of positive selection coinciding with the emergence of a pastoralist lifestyle on the Pontic-Caspian Steppe, and continued selection in the subsequent admixed post-Stone Age populations in Europe. This ultimately created a legacy of heterogeneity in MS risk observed across Europe today. These results address the long-standing debate around the north-south gradient in MS prevalence in Europe, and suggest that the Steppe ancestry gradient in modern populations - specifically at the HLA region - across the continent causes this phenomenon in combination with environmental factors. Furthermore, while epistasis between MS-associated variants in the HLA region has been demonstrated before[25, 26, 27, 28], we have shown that accounting for this explains 17% more variance than independent SNPs effects alone. Many of the haplotypes carrying these risk alleles have ancestry-specific origins, which could be exploited for individual risk prediction and may offer a pathway from ancestry associations into a mechanistic understanding of MS risk. We have contrasted these findings with results for rheumatoid arthritis (RA), another HLA class II associated chronic inflammatory disease, and found that the genetic risk for RA exhibits a contrasting pattern: genetic risk was highest in Stone Age hunter-gatherer ancestry and decreased over time.

Our interpretation of this history is that co-evolution between pathogens and their human hosts has resulted in massive and divergent ancestry-specific selection on immune response genes according to lifestyle and environment, driven by a range of pathogenic drivers, and "recombinant favouring selection" after these populations merged. The Late Neolithic and Early Bronze Age was a time of massively increased infectious diseases in human populations, due to increased population density as well as contact with, and consumption of, domesticated animals. Many diseases trace their origins to this period, such as tuberculosis (TB) caused by the intracellular bacteria *Mycobacterium tuberculosis* or *Mycobacterium bovis*[29, 30], bubonic plague caused by *Yersinia pestis*[31, 32, 33], herpes simplex virus[34], and chickenpox caused by varicella-zoster virus[35], and we have shown that many of the MS- and RA-associated variants under selection confer resistance to a range of infectious diseases and pathogens (Supplementary Note 8). For example, HLA-DRB1*15:01 is associated with protection against TB[36] and increased risk for lepromatous leprosy[37]. However, we are underpowered to detect specific associations beyond this hypothesis due to poor knowledge of the distribution and diversity of past diseases, poor preservation of endogenous pathogens in the archaeological record, and a lack of well-powered GWAS studies for many infectious diseases.

A pattern that repeatedly appears is that of lifestyle change driving changes in risk and phenotypic outcomes. We have shown that in the past environmental changes driven by lifestyle innovation inadvertently drove an increase in genetic risk for MS. Today, with increasing prevalence of MS cases

observed over the last five decades[38, 39]), we again observe a striking correlation with changes in our environment, including lifestyle choices and improved hygiene, which no longer favours this previous genetic architecture. Instead, the fine balance of genetically-driven cells within the immune system, which are needed to combat a broad repertoire of pathogens without harming self-tissue, has been met with new challenges, including a potential absence of requirement. For example, while a population of immune cells, T helper 1 (Th1), direct strong cellular immune responses against intracellular pathogens, T helper 2 (Th2) cells mediate humoral immune responses against extracellular bacteria and parasites and further have the capacity to guide the restoring of homeostasis,thus preventing damage of the infected tissue via immune-regulatory cytokines. We have shown that the majority of selected MS-associated SNPs are associated with protection against a wide range of pathogens, consistent with strong but balanced Th1/Th2 immunity in the Bronze age, where a diversification of pathogens likely took place. In contrast, although MS pathogenesis is complex and multicellular of nature, CD4+ Th cells, in particular IFN-ɣ producing Th1 cells and IL-17-producing Th17 cells play a key role in disease development[2]. The skewed Th1/Th2 balance observed in MS may partly result from the developed world's increased sanitation, which has led to drastically reduced burden of parasites, which the immune system had evolved to efficiently combat[40]. In the case of RA, the exposure of Hunter Gatherer populations to the respiratory or gastrointestinal pathogens linked to triggering RA[41] was likely low. The new pathogenic challenges associated with agriculture, animal domestication, pastoralism, and higher population densities might have substantially increased the risk of developing RA in genetically predisposed individuals, resulting in negative selection. If true, this would present a parallel between RA in the Bronze Age and MS today, in which lifestyle changes have exposed previously favourable genetic variants as autoimmune disease risks.

More broadly, it is clear that this was a critical period in human history during which highly genetically and culturally divergent populations evolved and eventually mixed. These separate histories dictate the genetic risk and prevalence of several autoimmune diseases today. Surprisingly, the emergence of the pastoralist Steppe lifestyle may have had an impact on immune response as great as or greater than the emergence of farming during the Neolithic transition, commonly held to be the greatest lifestyle change in human history.

DATA AVAILABILITY

All collapsed and paired-end sequence data for novel samples sequenced in this study will be made publicly available on the European Nucleotide Archive, together with trimmed sequence alignment map files, aligned using human build GRCh37. Previously published ancient genomic data used in this study are detailed in ST15, and are all already publicly available.

CODE AVAILABILITY

The modified version of CLUES used in this study is available from https://github.com/standard-aaron/clues. The pipeline and conda environment necessary to replicate the analysis of allele frequency trajectories and polygenic selection in Supplementary Note 6 are available on Github at https://github.com/ekirving/ms_paper. The code to create Ancestry Anomaly scores based on Chromosome painting is on Github at https://github.com/danjlawson/ms_paper. The codes to compute LDA and LDA score are available on Github at https://github.com/YaolingYang/LDAandLDAscore. The codes to implement HTRX and its simulation are on Github at https://github.com/YaolingYang/HTRX. The codes to implement ARS calculation are on Github at https://github.com/will-camb/ms_paper.

ACKNOWLEDGEMENTS

We extend our thanks to all the former and current staff at the Lundbeck Foundation GeoGenetics Centre and the GeoGenetics Sequencing Core, and to colleagues across the many institutions detailed below. We are particularly grateful to Maria Madrona, Lærke Hansen and Julie Bitz-Thorsen for laboratory assistance; and to Julie Hansen, Sandra Mularczyk, Katja Thorø Michler, Emilie Neerup Nielsen for their help with sampling, and to Line Olsen as project manager for the Lundbeck Foundation GeoGenetics Centre project. We thank UK Biobank Ltd. for access to the UK Biobank genomic resource. We are thankful to Illumina Inc. for collaboration. E.W. thanks St. John's College, Cambridge, for providing a stimulating environment of discussion and learning.

AUTHOR CONTRIBUTIONS

W.B., Y.Y., K.E.A., E.K.I-P, G.S., and L.T.J. contributed equally to this work.
A.I., D.J.L., L.F., and E.W. led the study.
W.B., A.R-M., L.F., R.N., and E.W. conceptualised the study.
R.N., K.K., L.F., and E.W. acquired funding for research.
A.R., C.G., F.D., M.L.S.J., S.B.M., B.S., L.K., I.M.H., N.W., L.V., and T.S.K., were involved in sample collection and processing
W.B., Y.Y., E.K.I-P, A.S., S.R., and D.J.L. were involved in developing and applying methodology.
W.B., Y.Y., E.K.I-P, G.S., A.A., A.R., E.A.D., M.S., S.R., A.I., and D.J.L. undertook formal analyses of data.
W.B., Y.Y., K.E.A., E.K.I-P, and L.T.J., A.I., L.F., and E.W. drafted the main text (W.B. led this).
W.B., Y.Y., E.K.I-P, G.S., L.T.J., E.A.D., A.S., F.D., M.L.S.J., S.B.M., B.S., L.K., I.M.H., N.W., L.V., A.I., and D.J.L. drafted supplementary notes and materials.
W.B., Y.Y., K.E.A., E.K.I-P, L.T.J., A.A., K.K., R.N., A.I., D.J.L., L.F., and E.W. were involved in reviewing drafts and editing.
All co-authors read, commented on, and agreed upon the submitted manuscript.

COMPETING INTERESTS

The authors declare no competing interests

Supplementary Figures

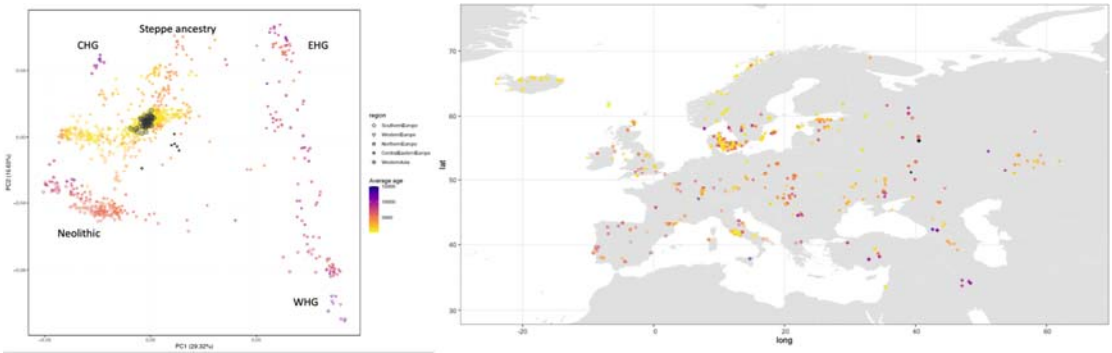

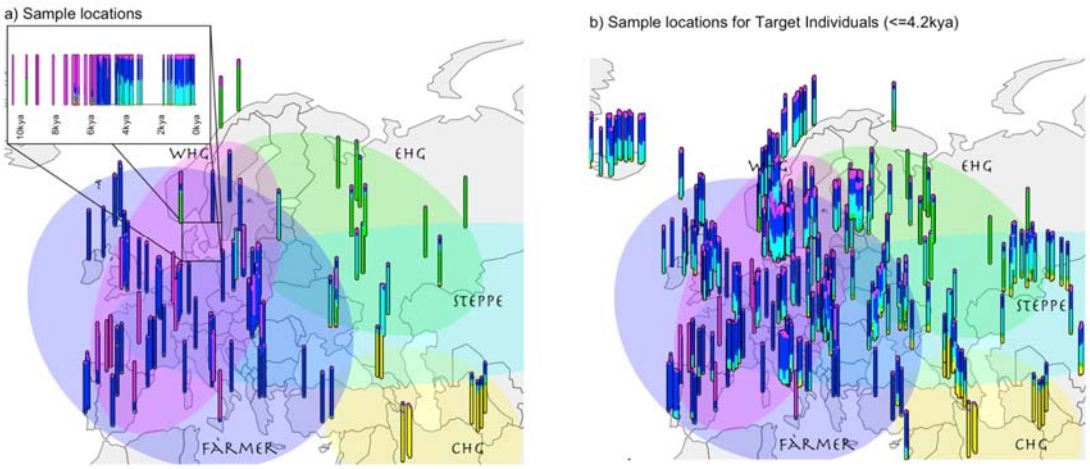

Supplementary Figure 1.1. Ancient sample PCA, map, ancestry proportions through time for samples in Denmark. (1) PC1 vs PC2 of the filtered Western Eurasian ancient samples included in this study. Black circled points are Danish Medieval and post-Medieval samples published here for the first time. Major component ancestry locations are labelled. (2) Map of ancient filtered Western Eurasian ancient samples included in this study (3a) Map of reference data and time transect of Denmark as in Figure 1. (3b) More recent ancient data (samples <4,200 years ago) not used as reference, showing the clines of the main ancestry components from (3a).

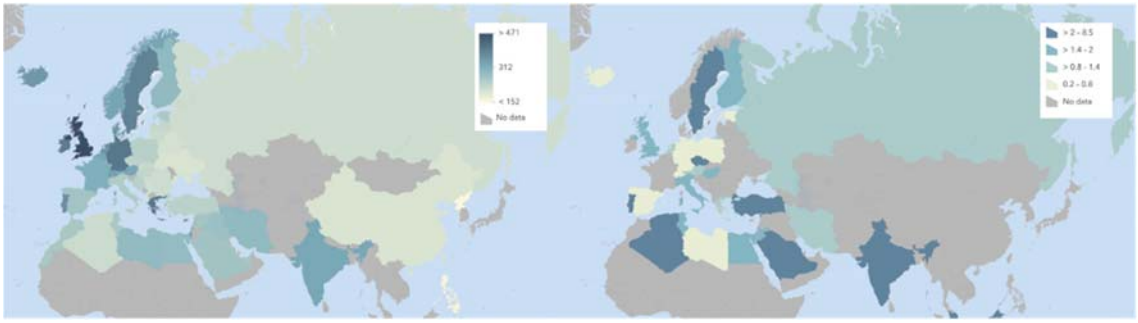

Supplementary Figure 1.2. Modern prevalences of RA (left) and CD (right).
Modern-day geographical distribution of RA and CD prevalence in Europe. Prevalence data for RA (cases per 100,000) was obtained from [42]. For CD, the seroprevalence (%) is based on the presence of transglutaminase and/or endomysial autoantibodies; data were obtained from [43].

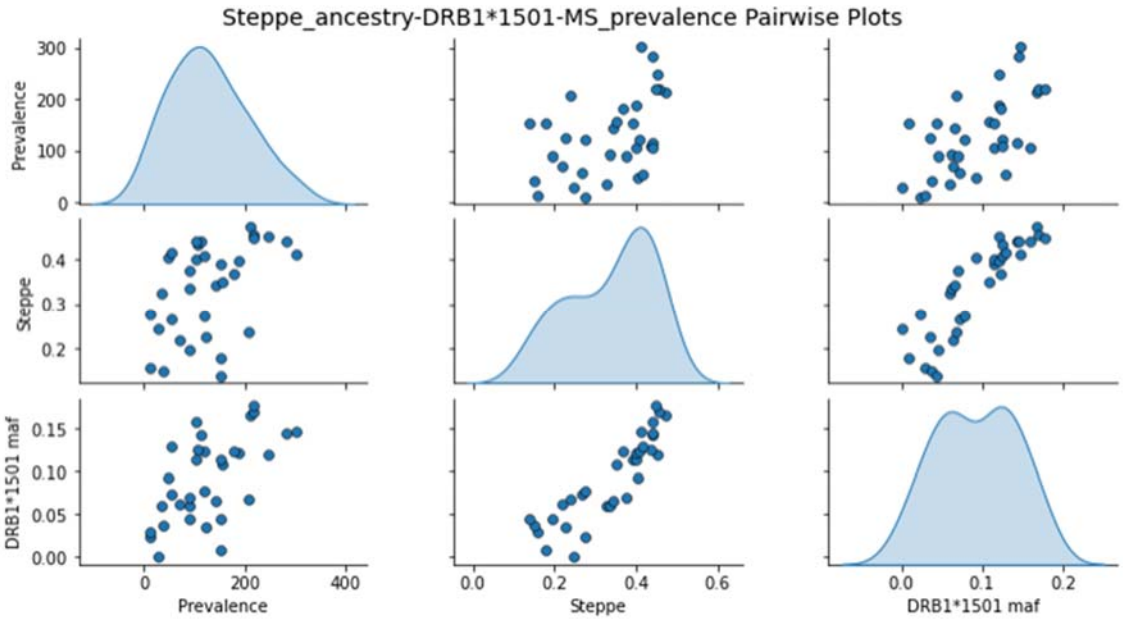

Supplementary Figure 1.3 Association between genome-wide Steppe ancestry, MS prevalence and DRB1*15:01 frequency in modern populations in the UK Biobank.

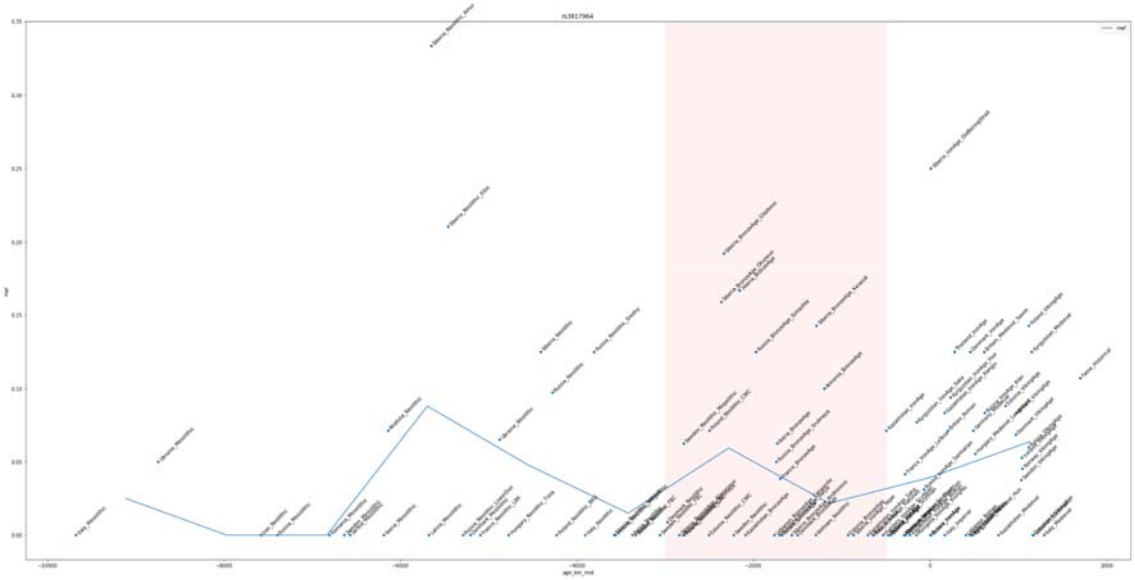

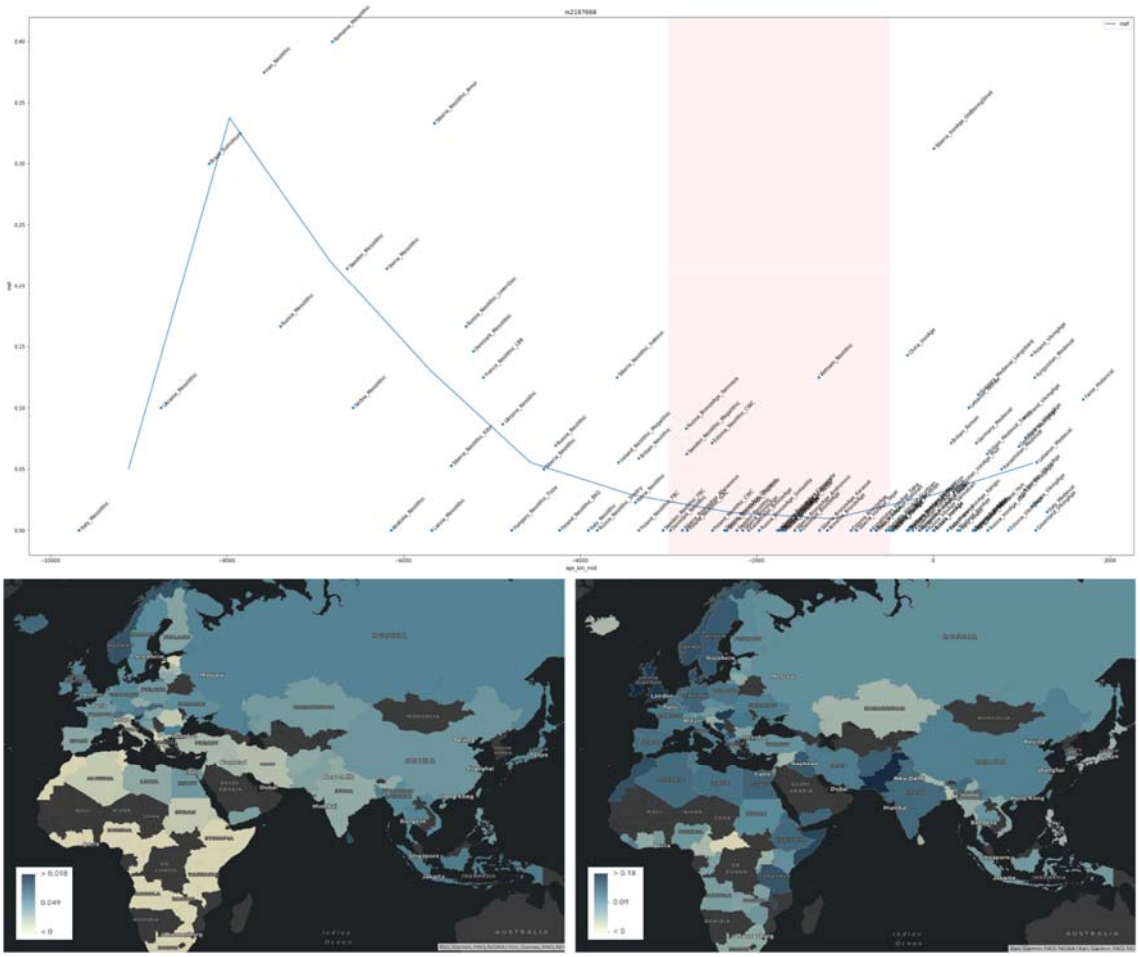

Supplementary Figure 2.1. Ancient and modern prevalences of HLA-DRB1*04:01 (rs3817964) and HLA-DQ2.5 (rs2187668).

Top and middle: Ancient distributions of HLA-DRB1*04:01, the largest genetic risk factor in RA, and HLA-DQ2.5, the largest genetic risk factor in CD. Average frequency across all populations is shown (blue line, 10 time bins) as well as the Bronze Age (red shading).

Bottom: Modern distribution of HLA-DRB1*04:01 (left) and HLA-DQ2.5 (right) in populations in the UK Biobank. NB the tag SNPs may be less effective at tagging these types in non-European populations, so we urge caution in interpretation - especially in African populations.

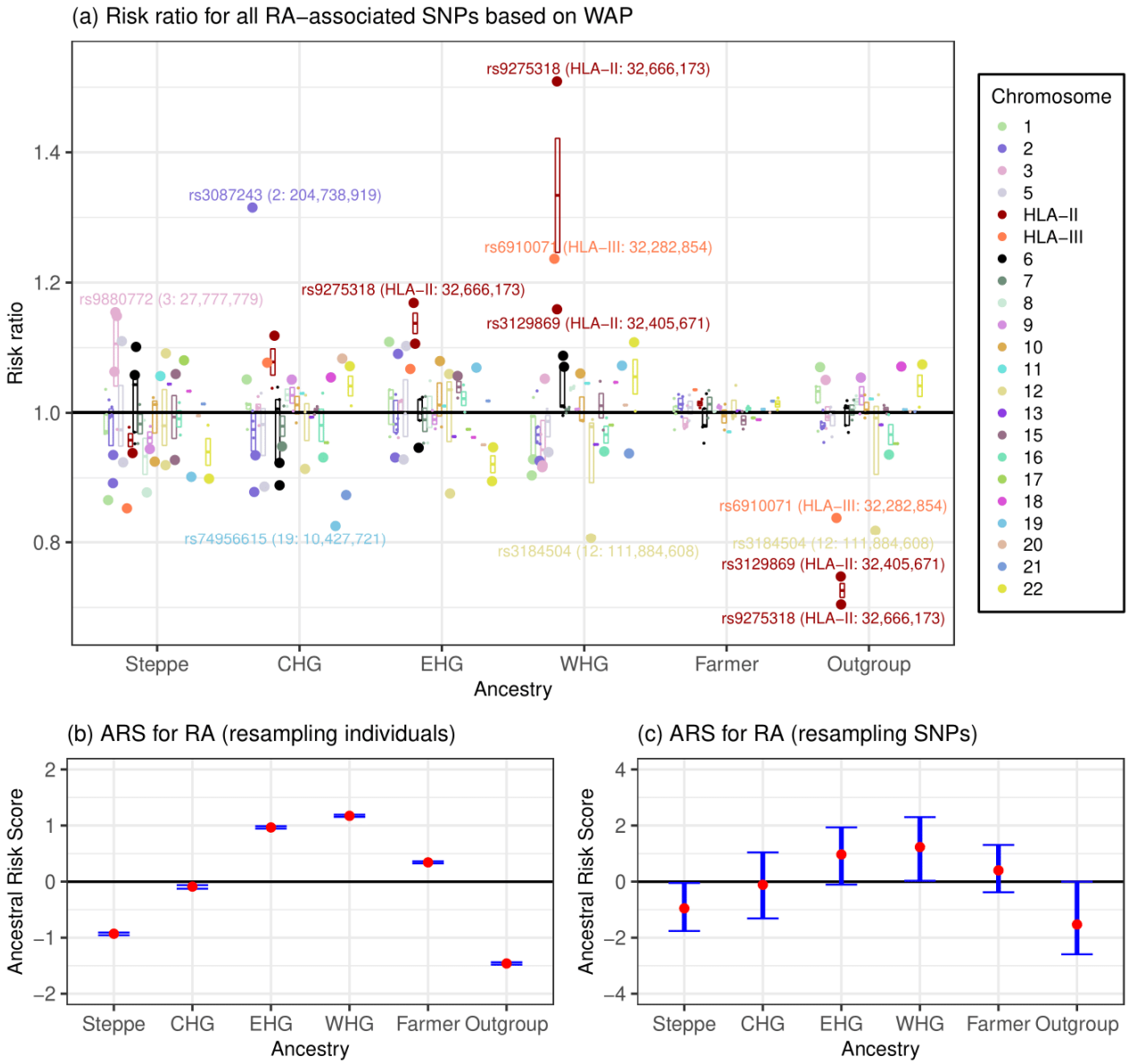

Supplementary Figure 3.1: Associations between local ancestry and RA in a modern population. a) Risk ratio of SNPs for RA based on weighted average prevalence (WAP; see Methods), when decomposed by inferred ancestry. Each ancestry is assigned a mean and confidence interval based on bootstrap resampling, for each chromosome (faded where non-significant). SNPs with risk ratio >1.15 or <0.85 are annotated. b-c) Genome-wide Ancestral Risk Scores (ARS, see Methods) for RA. Confidence intervals are estimated by either bootstrapping over individuals (b, which can be interpreted as testing power to reject a null of no association between RA and ancestry) and bootstrapping over SNPs (c, which can be interpreted as testing whether ancestry is associated with RA genome-wide).

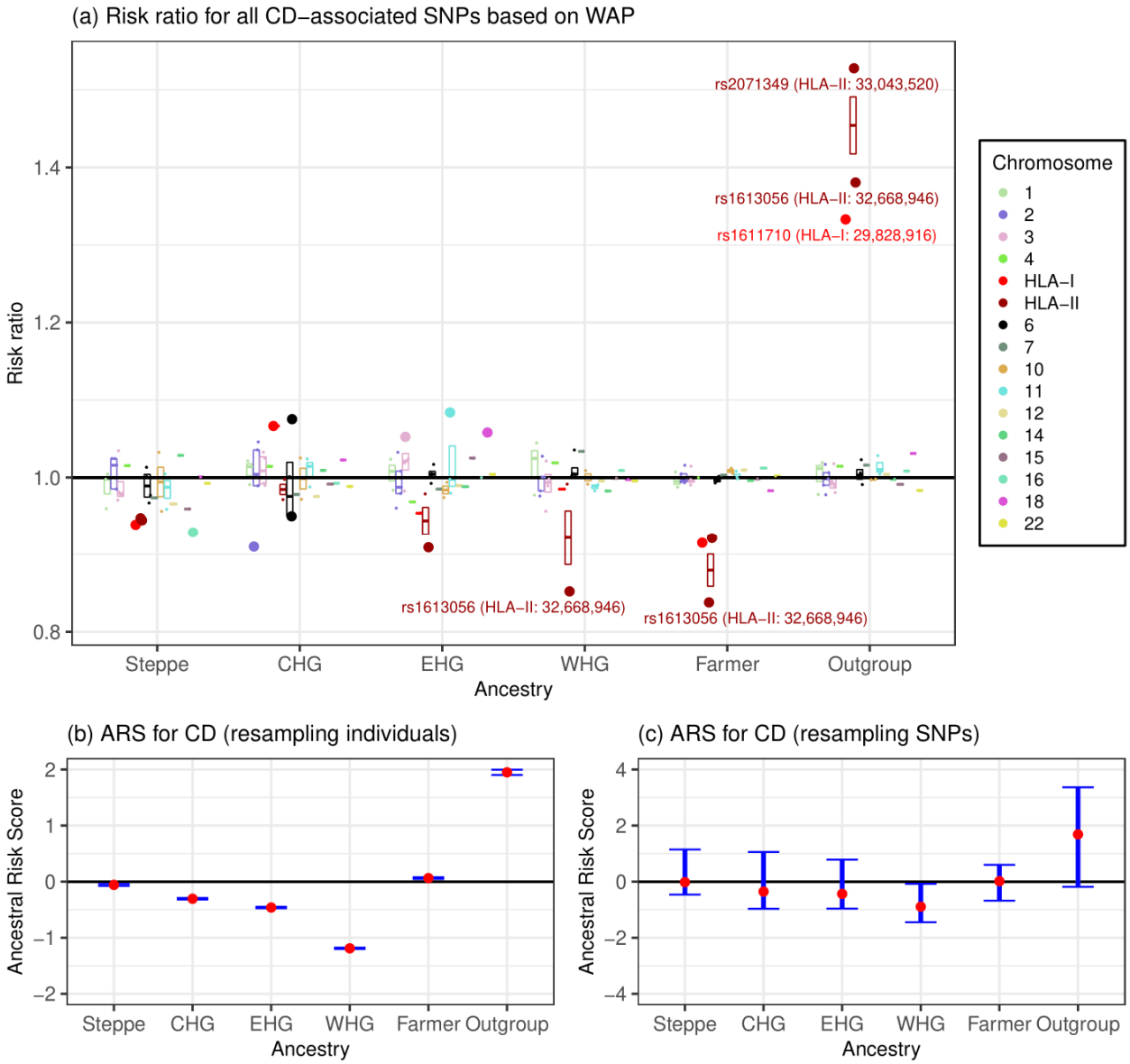

Supplementary Figure 3.2: Associations between local ancestry and CD in a modern population. a) Risk ratio of SNPs for CD based on weighted average prevalence (WAP; see Methods), when decomposed by inferred ancestry. Each ancestry is assigned a mean and confidence interval based on bootstrap resampling, for each chromosome (faded where non-significant). SNPs with risk ratio >1.15 or <0.85 are annotated. b-c) Genome-wide Ancestral Risk Scores (ARS, see Methods) for CD. Confidence intervals are estimated by either bootstrapping over individuals (b, which can be interpreted as testing power to reject a null of no association between CD and ancestry) and bootstrapping over SNPs (c, which can be interpreted as testing whether ancestry is associated with CD genome-wide).

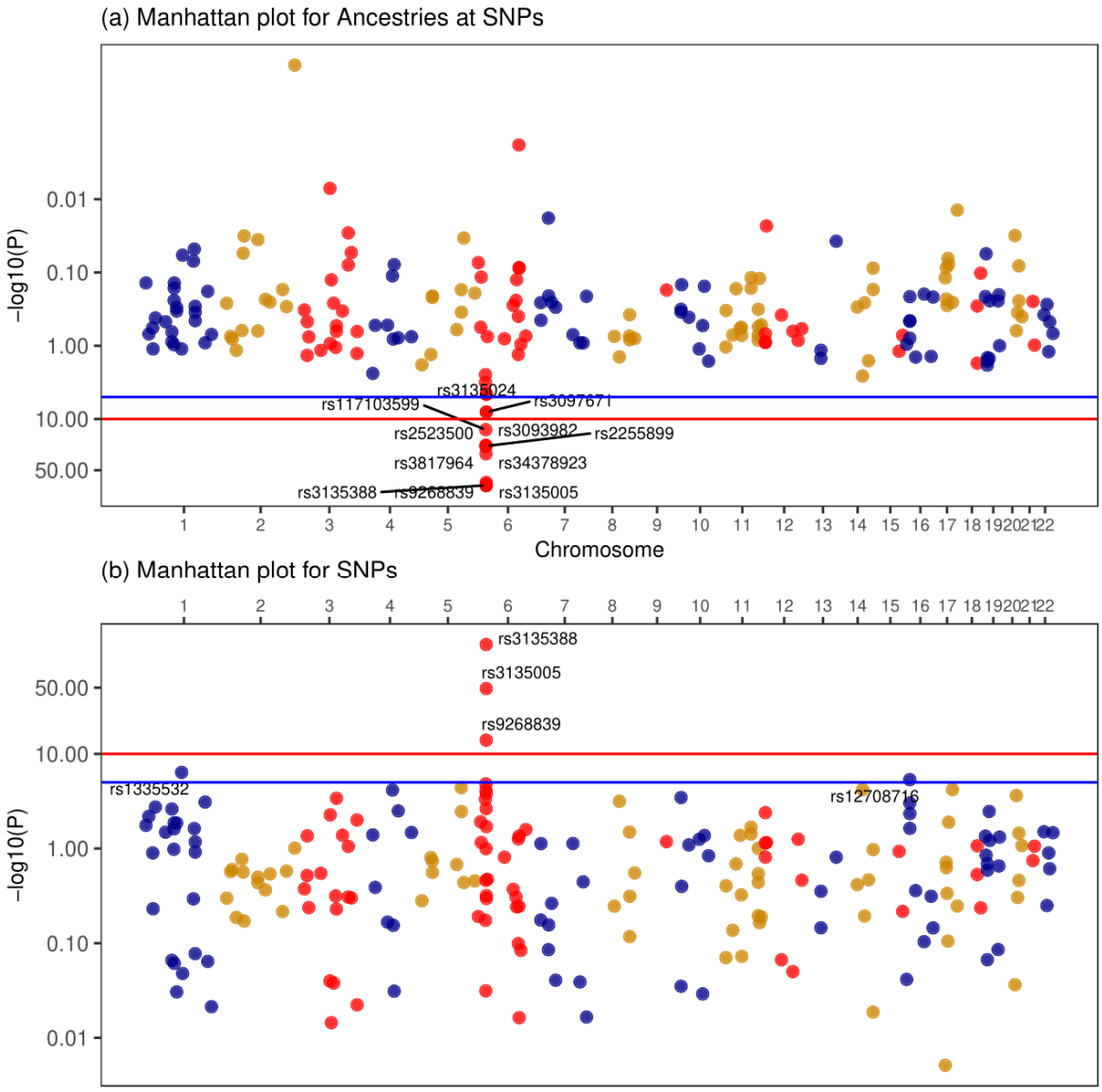

Supplementary Figure 4.1: Association with MS risk at externally ascertained SNPs, for (top) ancestry, and (bottom) SNPs.

Due to the UK Biobank being less powered (having fewer cases) than the Case-Control study from which these SNPs were found, the only statistically significant association is in the HLA.

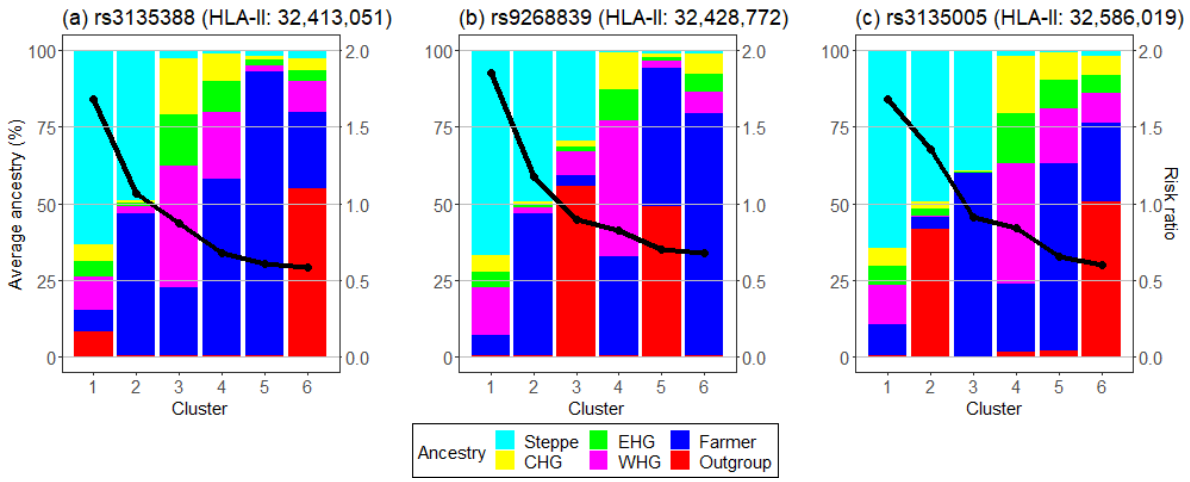

Supplementary Figure 4.2: Comparison between MS-risk and local ancestry for 3 example SNPs.

In the HLA class II region, all SNPs share a pattern in which high Steppe ancestry is associated with high MS-risk. The risk decreases monotonically and is not present in the Steppe precursor populations (Hunter Gathers), but is with the admixed Bronze-age European populations (Steppe + Farmer).

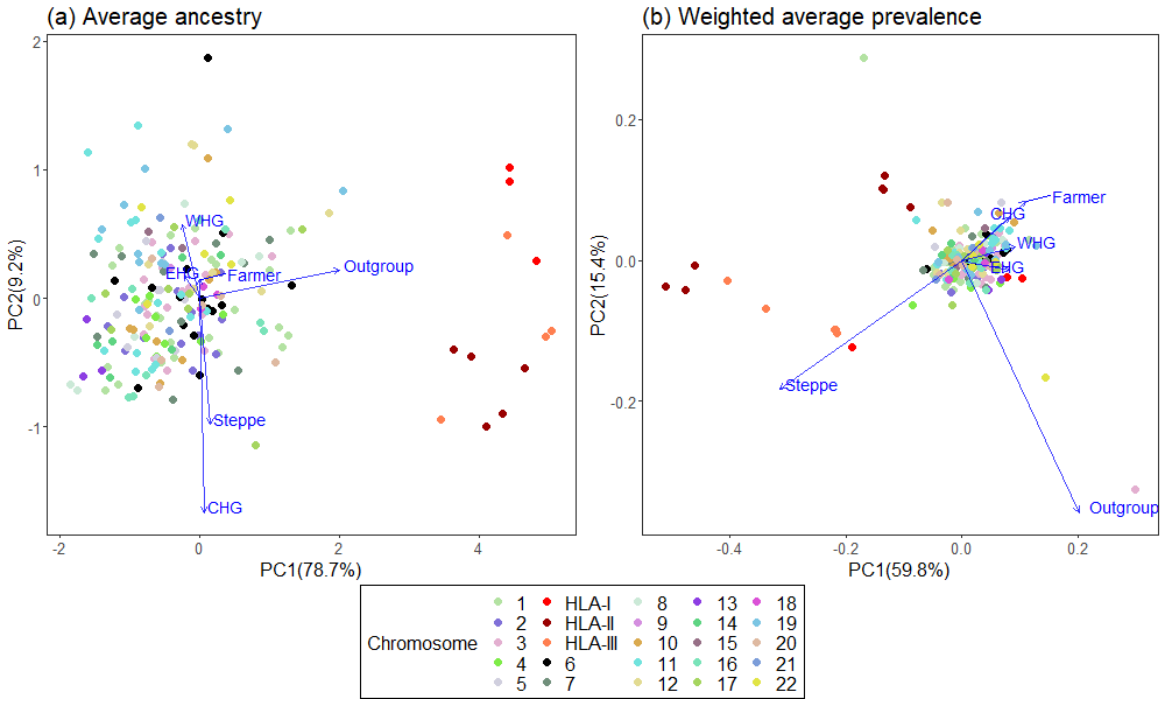

Supplementary Figure 4.3: Decomposition of individuals ancestry at MS risk SNPs in terms of (left) the ancestry of those SNPs alone, or (right) the Weighted average prevalence of MS in each ancestry after "logit" transformation.

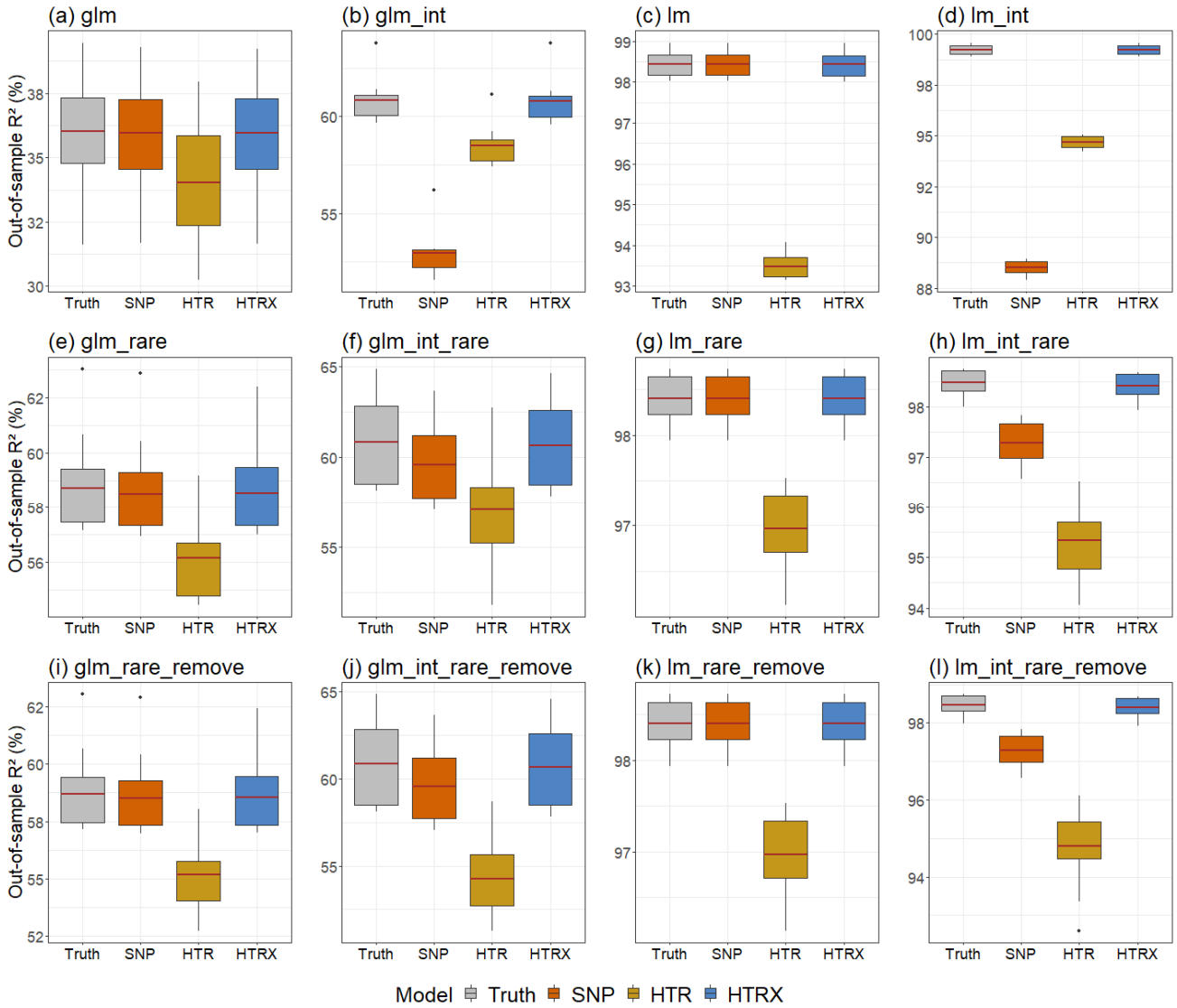

Supplementary Figure 4.4: Simulation study with four SNPs showing the boxplots of out-of-sample variance (with the red line representing the average) explained by HTRX compared to GWAS, HTR and the true model.

The total variance explained by HTRX is the same as SNP and bigger than HTR when there are no interactions. When interaction (with subtitle "int") exists, HTRX significantly outperforms GWAS and HTR. In all situations, HTRX works similarly to the truth.

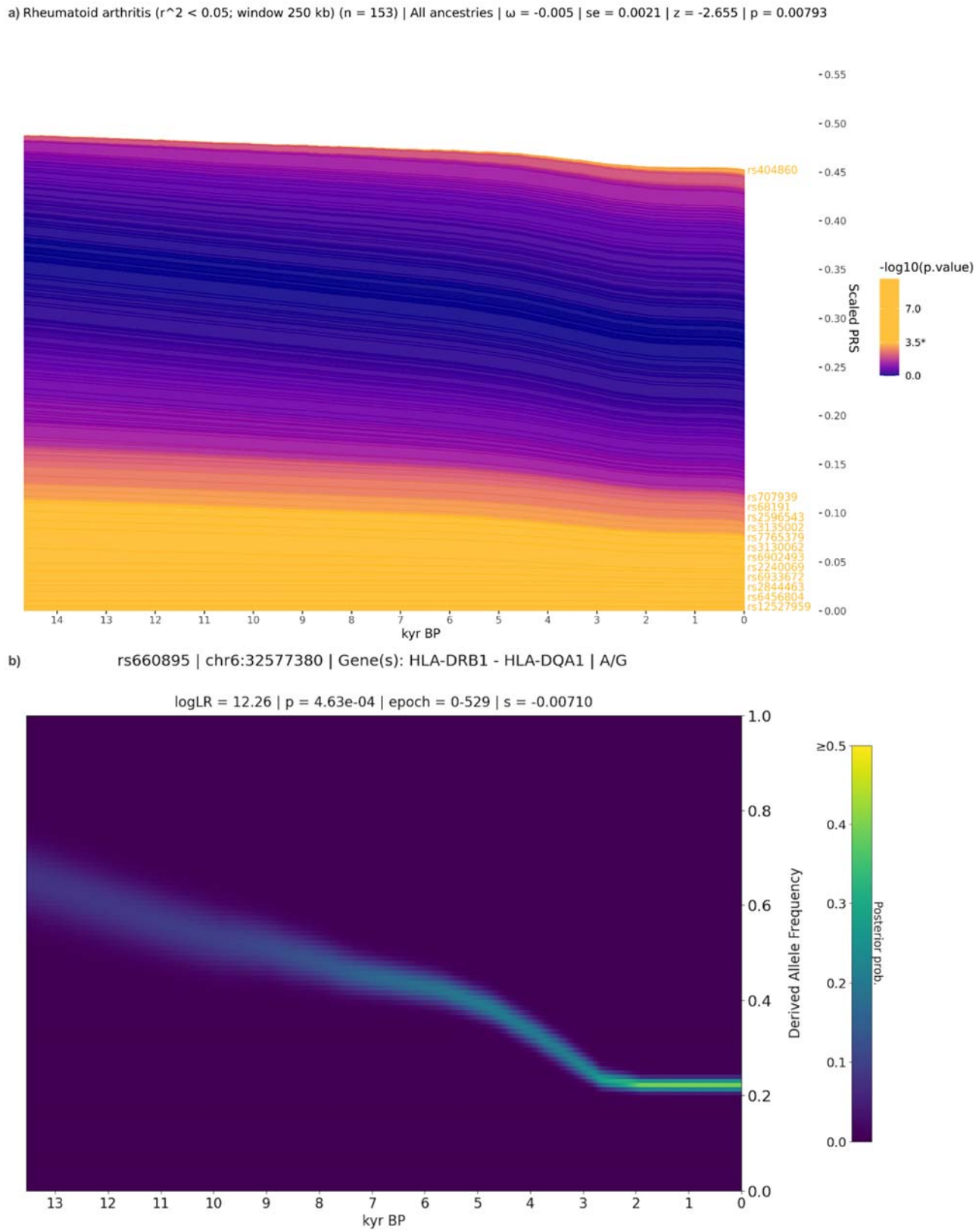

Supplementary Figure 5.1: Evidence for selection on RA-associated SNPs.
a) Stacked line plot of the pan-ancestry PALM analysis for RA, showing the contribution of alleles to disease risk over time. Individual SNPs are stacked, with their trajectories polarised to show the

frequency of the positive risk allele and weighted by their scaled effect size: when a given SNP bar becomes wider over time the risk allele has increased in frequency, and vice versa. SNPs are sorted by their marginal p-value and direction of effect, with selected SNPs that increase risk plotted on top. SNPs are also coloured by their marginal p-values, and significant SNPs are shown in yellow. The y-axis shows the scaled polygenic risk score (PRS), which ranges from 0 to 1, representing the maximum possible additive genetic risk in a population.
b) Posterior likelihood trajectory for rs660895, tagging HLA-DRB1*04:01, inferred by CLUES.

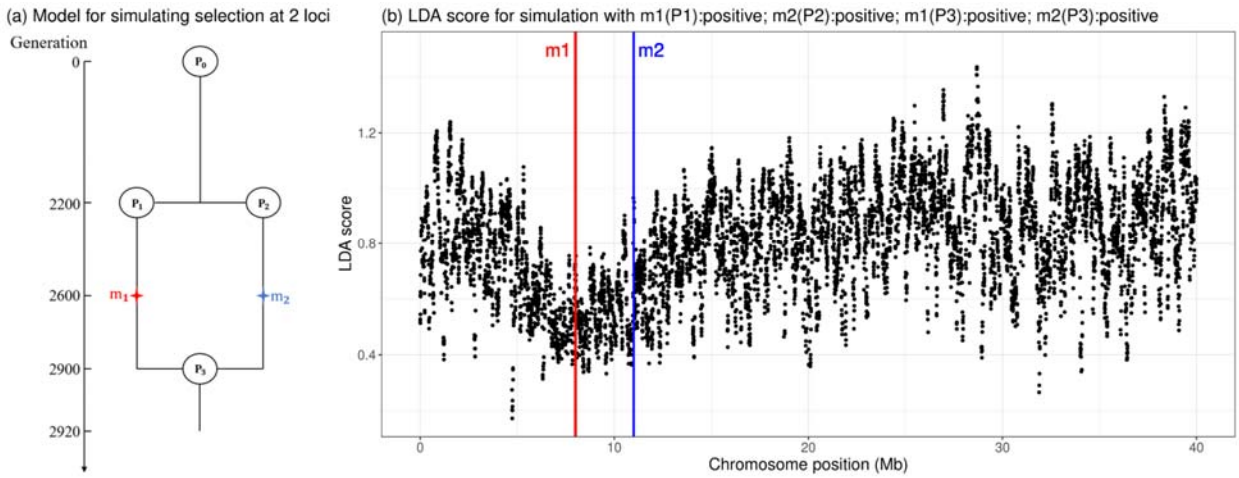

Supplementary Figure 6.1: Simulating Low LDA score.
Left: A simulated history in which a single population splits into two ("Steppe" and "Farmer") after 2200 generations and experiences positive selection on different loci (m_1 in P_1 and m_2 in P_2). After 2900 generations the populations merge ("Europeans") but selection continues on *both* loci.

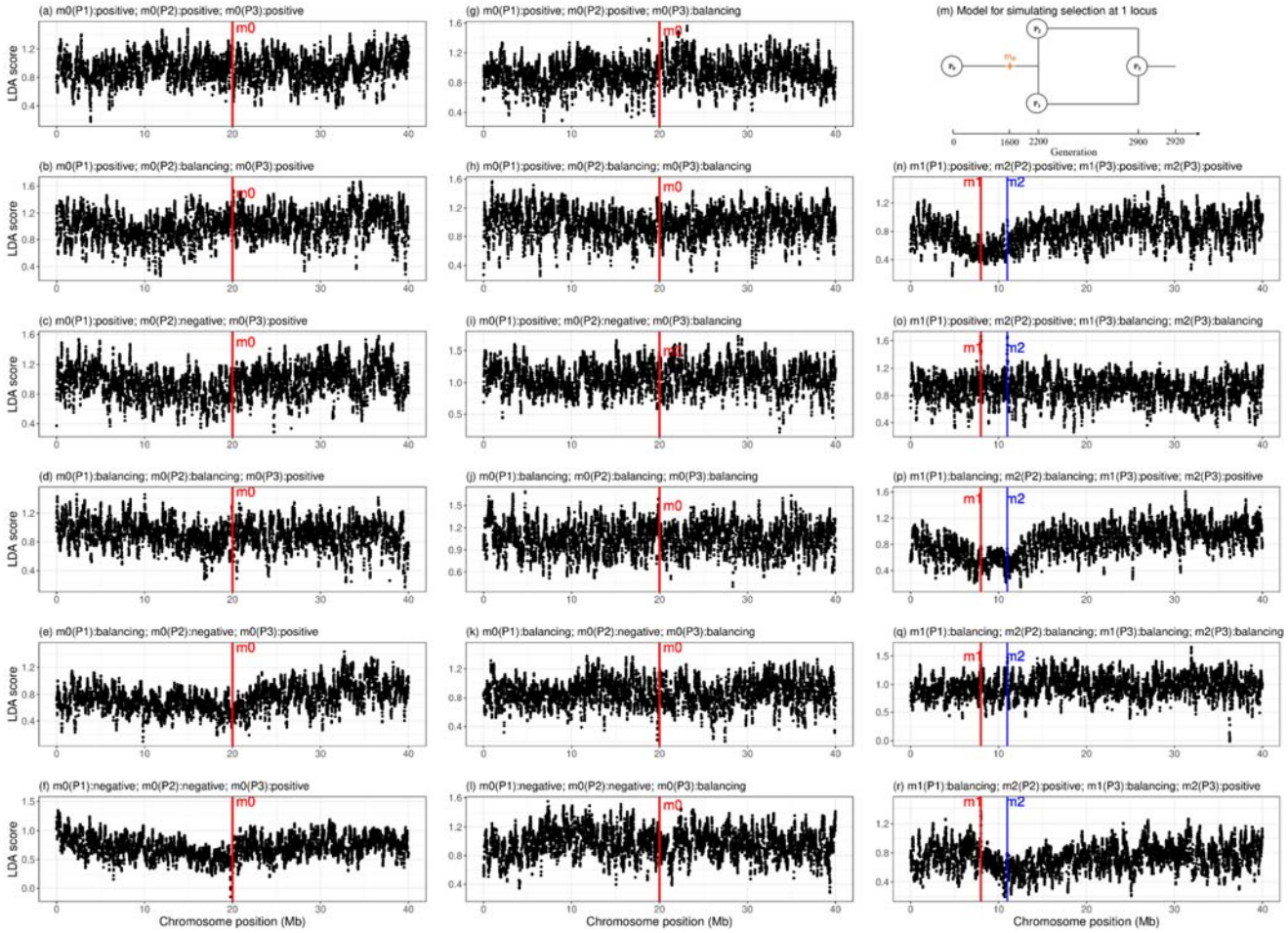

Supplementary Figure 6.2: LDAS simulation with positive or balancing selection in the modern population. The left two columns show simulations with a single variant satisfying the observed constraint that modern-day frequencies are not decreasing (i.e. not negative selection). The right column shows simulations with two variants, also obeying this constraint. The model for simulating 2 loci is the same as in Supplementary Figure 6.1, and that for 1 locus is in the top right of this plot (which differs only in the location of the selected variant in the separated populations).

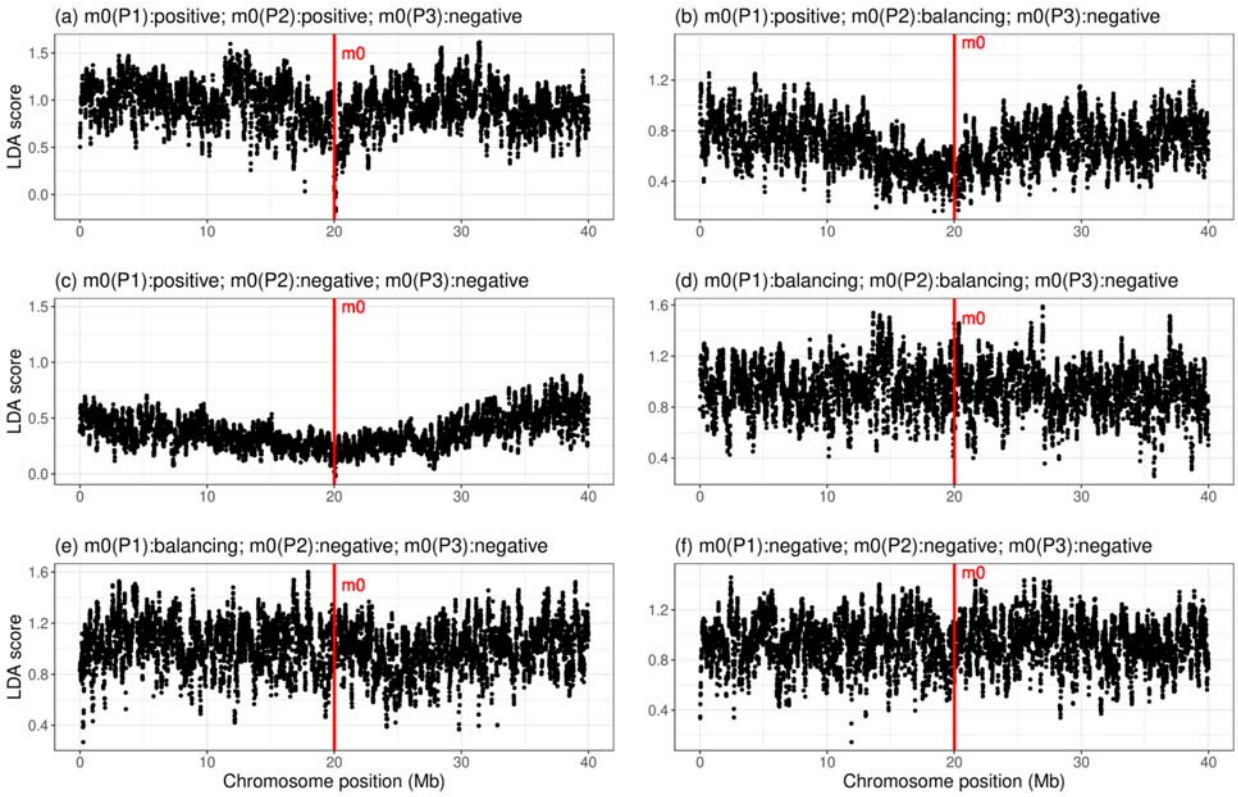

Supplementary Figure 6.3: LDAS simulation with single locus negatively selected in the modern population. In two cases this generates a low LDAS score, which requires recent negative selection (which is ruled out for HLA by the observed frequency trend). In this case, one ancestry dominates the region and recombination to the other conveys risk. The model used is in the top right of Supplementary Figure 6.2.

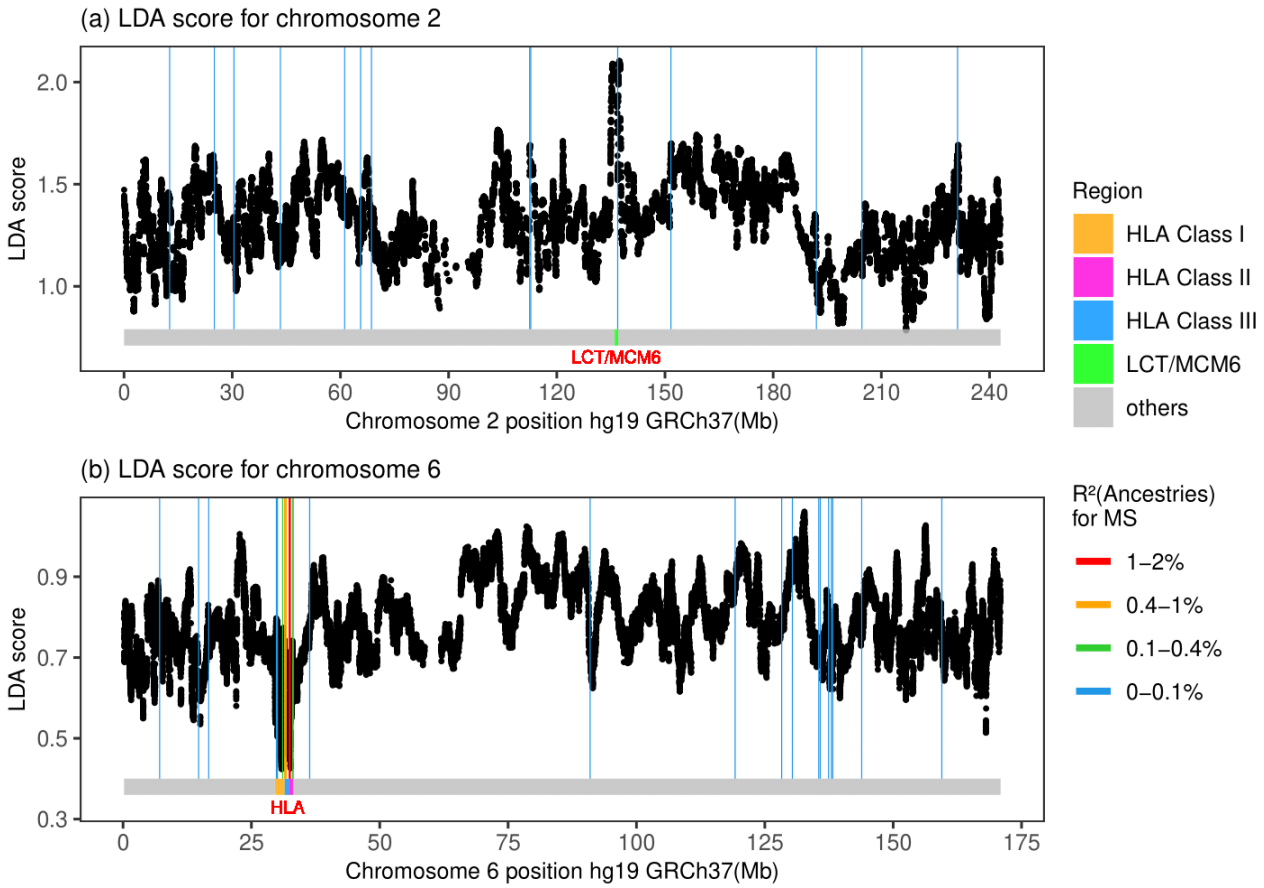

Supplementary Figure 6.4: LDAS on chromosome 6 and 2. LDA score is a) high in the LCT/MCM6 region while is b) low in the HLA region.

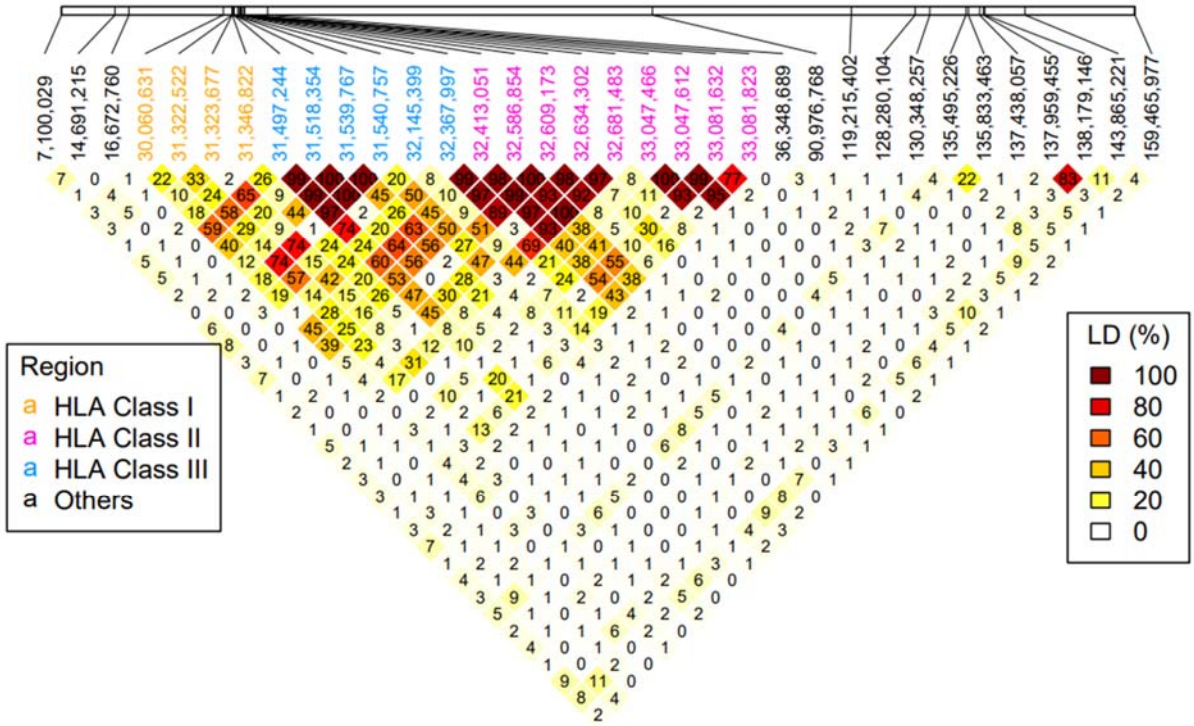

Supplementary Figure 6.5: Pairwise Linkage Disequilibrium (LD) plot (measured by D') for all the MS-associated SNPs on chromosome 6.

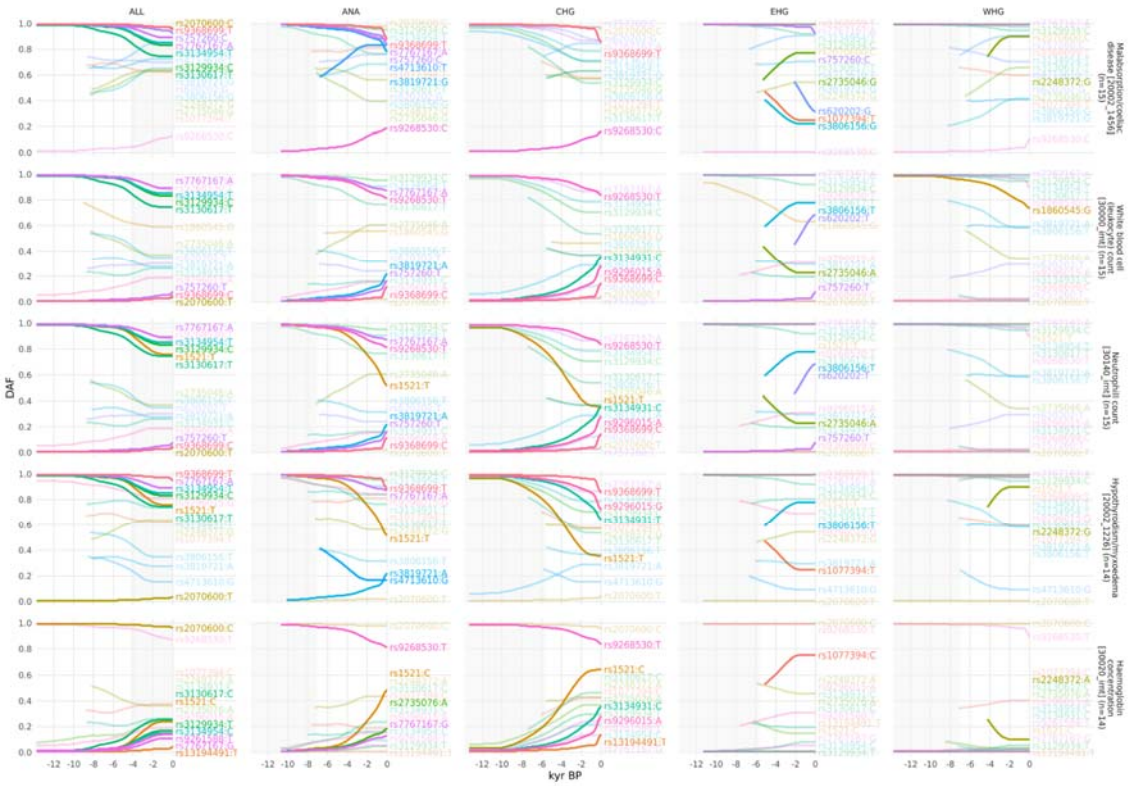

Supplementary Figure 7.1 Allele frequency plots for positively selected MS-associated SNPs that are also associated with other phenotypes in the UK Biobank. Traits 1-5.

SNPs are shown with their maximum likelihood trajectories, and polarised by the direction of their effect on the marginal UK Biobank trait (i.e. showing the 'risk' allele). Phenotypes are ordered according to the number of common SNPs, non-significant SNPs are shown with partial transparency, portions of the trajectory with low posterior density are cropped off, and the background is shaded for the approximate time period in which the ancestry existed as an actual population.

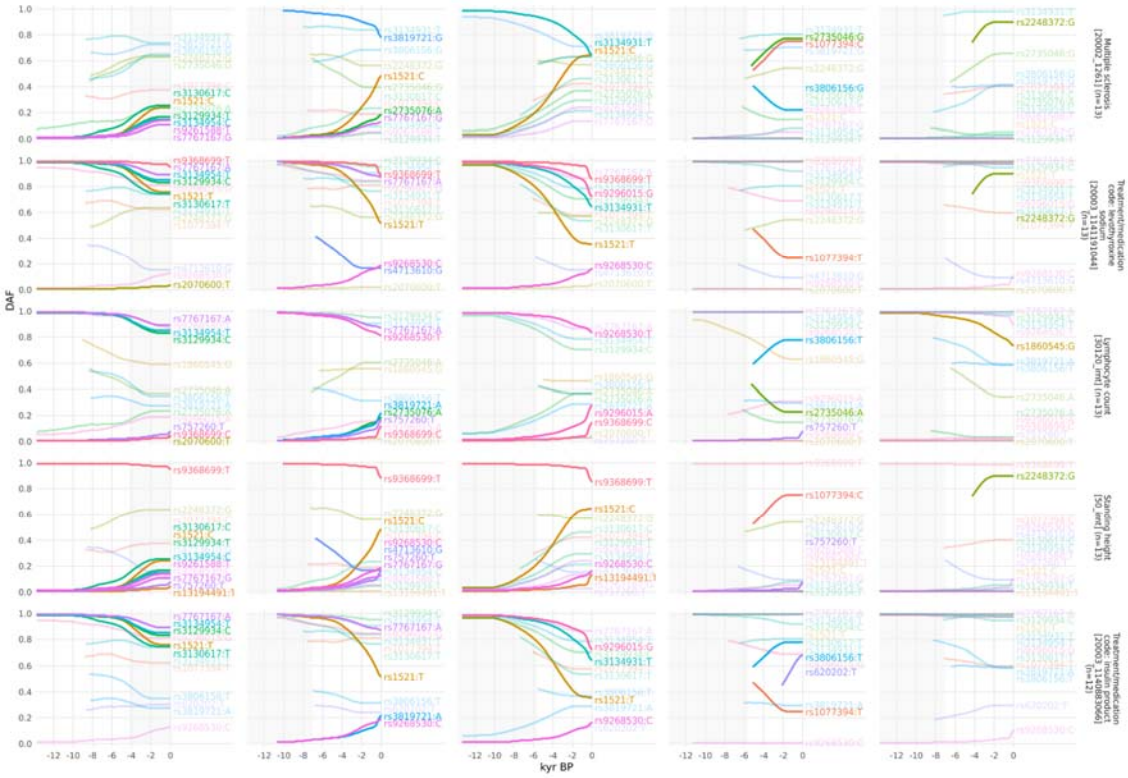

Supplementary Figure 7.2 Allele frequency plots for positively selected MS-associated SNPs that are also associated with other phenotypes in the UK Biobank. Traits 6-10.

SNPs are shown with their maximum likelihood trajectories, and polarised by the direction of their effect on the marginal UK Biobank trait (i.e. showing the 'risk' allele). Phenotypes are ordered according to the number of common SNPs, non-significant SNPs are shown with partial transparency, portions of the trajectory with low posterior density are cropped off, and the background is shaded for the approximate time period in which the ancestry existed as an actual population. Note that many phenotypes are underpowered in the UKBiobank GWAS, hence why MS appears as just the joint 7th in this list.

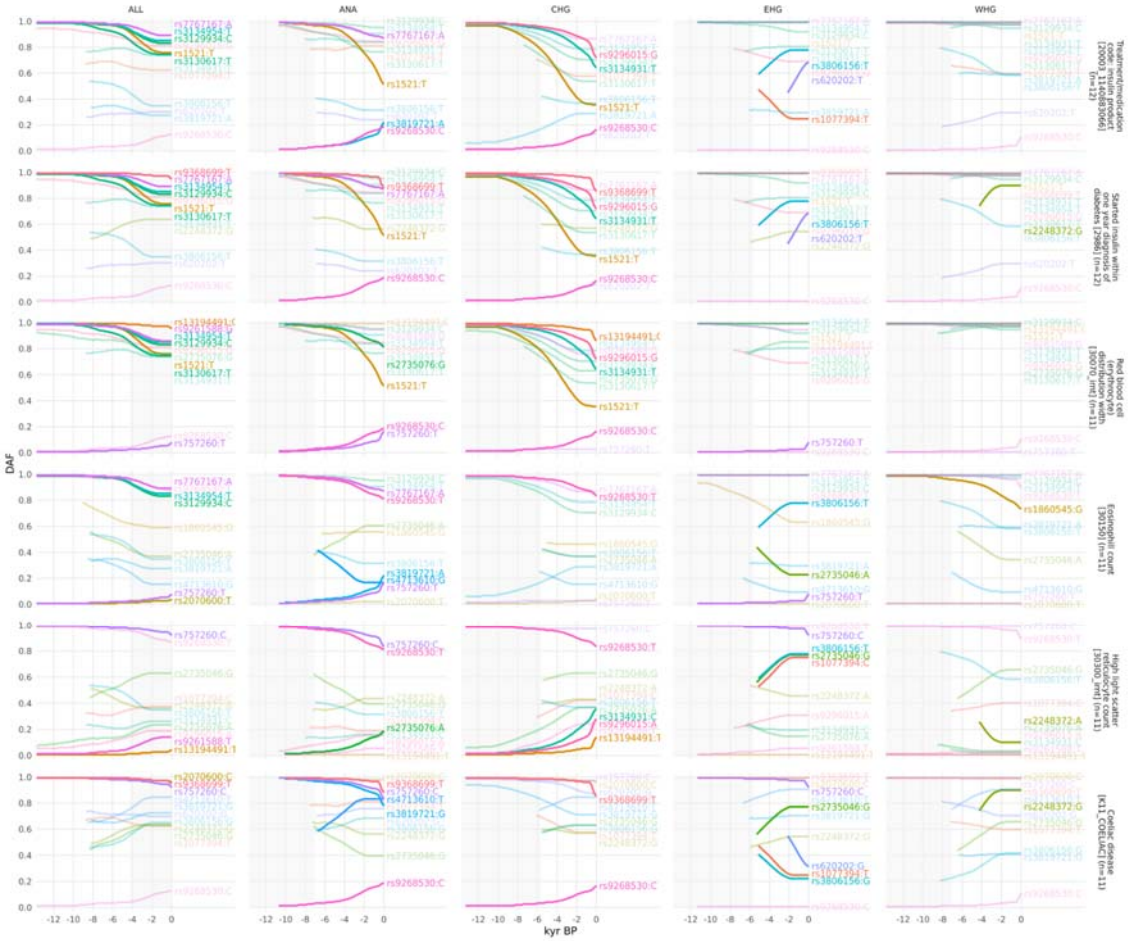

Supplementary Figure 7.3 Allele frequency plots for positively selected MS-associated SNPs that are also associated with other phenotypes in the UK Biobank. Traits 11-15.

SNPs are shown with their maximum likelihood trajectories, and polarised by the direction of their effect on the marginal UK Biobank trait (i.e. showing the 'risk' allele). Phenotypes are ordered according to the number of common SNPs, non-significant SNPs are shown with partial transparency, portions of the trajectory with low posterior density are cropped off, and the background is shaded for the approximate time period in which the ancestry existed as an actual population.

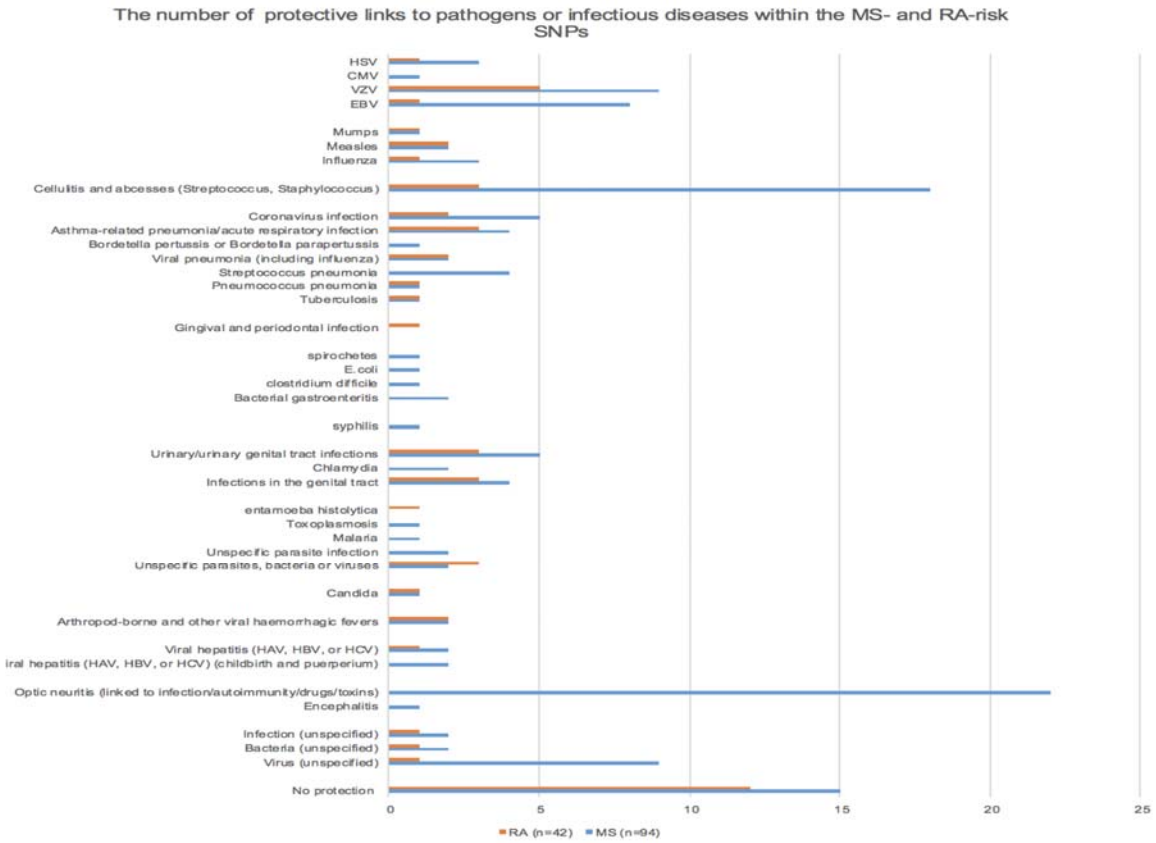

Supplementary Figure 8.1 The number of protective associations with pathogens or infectious diseases for the MA- and RA-associated selected SNPs

The number of protective associations to specific pathogens and/or diseases associated with the MS- and RA-SNPs that showed statistically significant evidence for selection using CLUES. One SNP can have a link to more than one pathogen and/or disease (see ST13 and ST14 for details on each SNP). Fifteen and twelve SNPs had no detectable links to any pathogen or infectious disease in the MS and RA SNP sets, respectively.

METHODS

Data Generation

Overview

In order to examine variants associated with phenotypes backwards in time, we assembled a large ancient DNA dataset. Here we present new genomic data from 86 ancient individuals from Medieval and post-Medieval periods from Denmark (Supplementary Figure 1, Supplementary Note 1, ST1). The samples range in age from around the XIth to the XVIIIth century. We extracted ancient DNA from tooth cementum or petrous bone and shotgun sequenced the 86 genomes to a depth of genomic coverage ranging from 0.02 X to 1.6 X (mean = 0.39 X and median = 0.27 X). The genomes of the new 86 individuals were imputed using the 1,000 Genomes phased data as a reference panel by an imputation method designed for low coverage genomes (GLIMPSE[44]), and we also imputed 1,664 ancient genomes presented in the accompanying study 'Population Genomics of Stone Age Eurasia'[9]. Depending on the specific data quality requirements for the downstream analyses, we filtered out samples with poor coverage, variant sites with low MAF and with low imputation quality (average

genotype probability < 0.98). Our dataset of ancient individuals span approximately 15,000 years across Eurasia (Supplementary Figure 1).

Ancient data DNA extraction and library preparation

Laboratory work was conducted in the dedicated ancient DNA clean-room facilities at the Lundbeck Foundation GeoGenetics Centre (Globe Institute, University of Copenhagen). A total of 86 Medieval and post-Medieval human samples from Denmark (ST2) were processed using semi-automated procedures. Each sample was processed in parallel. For each extract non USER-treated and USER-treated (NEB) libraries were built[45]. All libraries were sequenced on the NovaSeq6000 instrument at the GeoGenetics Sequencing Core, Copenhagen, using S4 200 cycles kits version 1.5. A more detailed description of DNA extraction and library preparation can be found in Supplementary Note 1.

Basic bioinformatics

The sequencing data was demultiplexed using the Illumina software BCL Convert (https://emea.support.illumina.com/sequencing/sequencing_software/bcl-convert.html, Illumina Inc.) . Adapter sequences were trimmed and overlapping reads were collapsed using AdapterRemoval (2.2.4[46]). Single-end collapsed reads of at least 30bp and paired-end reads were mapped to the human reference genome build 37 using bwa (0.7.17[47]) with seeding disabled to allow for higher sensitivity. Paired- and single-end reads for each library and lane were merged, and duplicates were marked using Picard MarkDuplicates (2.18.26, http://picard.sourceforge.net) with a pixel distance of 12000. Read depth and coverage were determined using samtools (1.10[48]) with the all sites used in the calculation (-a). Data was then merged to sample level and duplicates were marked again.

DNA authentication

In order to determine the authenticity of the ancient reads, post-mortem DNA damage patterns were quantified using mapDamage2.0[49]. Next, two different methods were used to estimate the levels of contamination. Firstly, we applied ContamMix in order to quantify the fraction of exogenous reads in the mitochondrial reads by comparing the mtDNA consensus genome to possible contaminant genomes[50]. The consensus was constructed using an in-house perl script that used sites with at least 5x coverage, and bases were only called if observed in at least 70% of reads covering the site. Lastly, we applied ANGSD (0.931[51]) to estimate nuclear contamination by quantifying heterozygosity on the X chromosome in males. Both contamination estimates only used filtered reads with a base quality of ≥20 and mapping quality of ≥30.

Imputation

We combined the 86 newly sequenced Medieval and post-Medieval Danish individuals with 1,664 previously published ancient genomes[9]. We then excluded individuals showing: contamination (more than 5%); low autosomal coverage (less than 0.1 X); low genome-wide average imputation genotype probability (less than 0.98), and we chose the best quality sample in a close relative pair (first or second degree relative). A total of 1,557 individuals passed all filters, and were used in downstream analyses. We restricted the analysis to SNPs with imputation INFO score ≥ 0.5 and MAF ≥ 0.05.

Kinship analysis and uniparental haplogroup inferences

READ[52] was used to detect the degree of relatedness between pairs of individuals.

The mtDNA haplogroups of the Medieval and post-Medieval individuals were assigned using HaploGrep2[53]. Y chromosome haplogroup assignment was inferred following the workflow already published[54]. More details can be found in Supplementary Note 2.

Population genetic analyses

We used principal component analysis (PCA) (Supplementary Figure 1.1) to investigate the overall population structure of the dataset. We used plink[55], excluding SNPs with minor allele frequency (MAF) < 0.05 in the imputed panel. Based on 1,210 ancient western Eurasia imputed genomes, the Medieval and post-Medieval samples cluster very close to each other, displaying a relatively low genetic variability and situated within the genetic variability observed in the post-Bronze Age western Eurasian populations.

We used three methods to estimate ancestry components in our ancient samples: model-based clustering (ADMIXTURE[56]) (Supplementary Note 1, Figure S1.1) on a subset of 826,248 SNPs; qpAdm[57] (Supplementary Note 1 Figure S1.2 and Table S1.1) with a reference panel of three genetic ancestries (WHG, Neolithic Farmer, and Steppe) on the same 826,248 SNPs. We performed qpAdm applying the option “allsnps: YES” and a set of 7 outgroups was used as "right populations": Siberia_UpperPaleolithic_UstIshim, Siberia_UpperPaleolithic_Yana, Russia_UpperPaleolithic_Sunghir, Switzerland_Mesolithic, Iran_Neolithic, Siberia_Neolithic, USA_Beringia. We set a minimum threshold of 100,000 SNPs and only results with $p > 0.05$ only have been considered. Finally we ran chromosome painting[58] using a panel of 7 ancestries (as on the UK Biobank). We ran chromosome painting on all ancient individuals not in the reference panel, using a reference panel of ancient donors grouped into populations to represent specific ancestries: western hunter-gatherer (WHG), eastern hunter-gatherer (EHG), Caucasus hunter-gatherer (CHG), Neolithic Farmer, Yamnaya, African and EastAsian (method described in [9] Supplementary Note 3h). Painting followed the pipeline of [59] based on GLOBETROTTER[60], with admixture proportions estimated using Non-Negative Least squares. We also painted individuals born in Denmark of a typical ancestry based on density-based clustering of the first 18 PCs[9]. This generated both local ancestry probabilities and genome-wide ancestry fractions for each painted individual. The reference panel used for chromosome painting was designed to capture the various components of European ancestry only, and so we urge caution in interpreting these results for non-European samples.

This dataset provides the opportunity to study the population history of Denmark from the Mesolithic to the post-Medieval period, covering around 10,000 years, which can be considered a typical Northern European population. Our results clearly demonstrate the impact of previously described demographic events, including the influx of Neolithic Farmer ancestry ~9,000 years ago and Steppe ancestry ~5,000 years ago[12, 10]. We highlight genetic continuity from the Bronze Age to the post-Medieval period (Supplementary Note 1 Figure S1.1), although *qpAdm* detected a small increase in the Neolithic Farmer component during the Viking Age (Supplementary Note 1 Figure S1.2 and Table S1.1), while the Medieval period marked a time of increased genetic diversity, likely reflecting increased mobility across Europe. This genetic continuity is further confirmed by the haplogroups identified in the uniparental genetic makers (Supplementary Note 2). Together, these results suggest that after the Bronze Age Steppe migration there was no other major gene flow into Denmark from populations with significantly different Neolithic and Bronze Age ancestry compositions, and therefore no changes in these ancestry components in the Danish population.

Local ancestry

We used two estimates of local ancestry from [9]: (1) first coalescent labels generated by running Chromopainter[58] on all "White British" individuals in the UK Biobank, using the same reference panel described above. Henceforth 'local ancestry'. (2) Ancestry path labels in GBR, FIN and TSI 1000G populations[61]) and 1015 ancient genomes generated using a neural network to assign ancestry paths based on a sample's nearest neighbours at the first five informative nodes of a marginal tree sequence, where an informative node is defined as one which has at least one leaf from the reference set of ancient samples described above ([9] Supplementary Note S3i). Henceforth 'ancestry path labels'.

SNP associations

We aimed to generate SNP associations from previous studies for each phenotype in a consistent approach. To generate a list of SNPs associated with multiple sclerosis (MS), rheumatoid arthritis (RA) and celiac disease (CD), we used two approaches: in the first, we downloaded fine-mapped SNPs from previous association studies. For each fine-mapped SNP, if the SNP did not have an ancestry path label, we found the SNP in highest LD that did, with a minimum threshold of $r^2 \geq 0.7$ in the GBR, FIN and TSI 1000G populations using LDLinkR[62]. The final SNPs used for each phenotype can be found in ST4 (MS), ST5 (RA), and ST6 (CD).

For MS, we used data from [3]. For non-MHC SNPs, we used the 'discovery' SNPs with P(joined) and OR(joined) generated in the replication phase. For MHC variants, we searched the literature for the reported HLA alleles and amino-acid polymorphisms (ST3). In total, we generated 205 SNPs which were either fine-mapped or in high LD with a fine-mapped SNP (15 MHC, 190 non-MHC).

For RA, we downloaded 57 genome-wide significant non-MHC SNPs for seropositive RA in Europeans[63]. We retrieved MHC associations separately ([64], with associated ORs and p-values from [65]). In total, we generated 51 SNPs which were either fine-mapped or in high LD with a fine-mapped SNP (3 MHC, 48 non-MHC).

For CD, we retrieved non-MHC SNPs from [66]. We used MHC SNPs from [67], with associated ORs and p-values from [68]. In total, this generated 32 SNPs which were either fine-mapped or in high LD with a fine-mapped SNP (3 MHC, 29 non-MHC).

Secondly, because we could not always find tag SNPs for fine-mapped SNPs that were present in our ancestry path labels dataset, we found that we were losing significant signal from the HLA, therefore we generated a second set of SNP associations. We downloaded full summary statistics for each disease (MS: [3]; RA: [69], CD: http://www.nealelab.is/uk-biobank/), restricted to sites present in the ancestry path labels dataset, and ran Plink's (PLINK v1.90b4.4[70]) clump method (parameters: --clump-p1 5e-8 --clump-r2 0.05 --clump-kb 250 as in [71] using LD in the GBR, FIN and TSI 1000G populations[61] to extract genome-wide significant independent SNPs.

In the main text we report results for the first set of SNPs ('fine-mapped') for analyses involving local ancestry in modern data, and the second set of SNPs ('pruned') for analyses involving polygenic measures of selection (CLUES/PALM).

REGIONS OF UNUSUAL ANCESTRY AND GENE ENRICHMENT

To assess which regions of ancestry were unusual, we converted the ancestry estimates to a Z-score. Specifically, we let $A(i,j,j)$ denote the probability of the kth ancestry ($k = 1,\ldots,K$) at the jth SNP ($j = 1,\ldots,J$) of a chromosome for the ith individual ($i = 1,\ldots,N$). We then computed the mean

painting for each SNP, $A(j,k) = \frac{1}{N}\sum_{i=1}^{N} \quad A(i,j,k)$. From this we estimated a scale parameter μ_k and deviation parameter σ_k using a block-median approach. Specifically we partitioned the genome into 0.5Mb regions, and within each, computed the mean and standard deviation of the ancestry. The parameter estimates are then the median values over the whole genome. We then computed an anomaly score for each SNP for each ancestry $Z(j,k) = (A(j,k) - \mu_k)/\sigma_k$.

To arrive at an anomaly score for each SNP aggregated over all ancestries, we also had to account for correlations in the ancestry paintings. Instead of scaling each ancestry deviation $A^*(j,k) = A(j,k) - \mu_k$ by its standard deviation, we instead "whitened" them, i.e. rotated the data to have an independent signal. Let $C = A^{*T}A^*$ by a $K \times K$ covariance matrix, and let $C^{-1} = UDV^T$ be the Singular Value Decomposition. Then $W = UD^{1/2}$ is the whitening matrix from which $Z = A^*W$ are normally distributed with covariance matrix diag(1) under the null that A^* is normally distributed with mean 0 and unknown covariance Σ. The "ancestry anomaly score" test statistic for each SNP is $t(j) = \sum_{k=1}^{K} \quad Z(j,k)^2$, which is Chi-squared distributed with K degrees of freedom under the null, and we reported p-values from this.

To test for gene enrichment we formed a list of all SNPs reaching genome-wide significance ($p < 5^{-8}$) and using the R package *gprofiler2*[72] converted these to a unique list of genes. We then used *gost* to perform an enrichment test for each GO term, for which we used default p-value correction via the *g:Profiler SCS* method. This is an empirical correction based on performing random lookups of the same number of genes under the null, to control the error rate and ensure that 95% of reported categories (at p=0.05) are correct.

ALLELE FREQUENCY PLOTS OVER TIME

To investigate how effect allele frequencies have changed over time, we extracted high effect alleles for each phenotype from the ancient data. We excluded all non-Eurasian samples, grouped them by 'groupLabel', excluded any group with fewer than 4 samples, and coloured points by ancestry proportion according to genome-wide NNLS based on chromosome painting (above).

CLUSTER ANALYSIS

In order to understand whether risk-conferring haplotypes evolved in the Steppe population, or in a pre- or post-dating population in which Steppe ancestry is high, we used k-means clustering on the dosage of each ancestry for each selected significant SNP and investigated the dosage distribution of clusters with significantly higher MS prevalence. For the target SNPs, the Elbow method[73]. suggested selecting around 5-7 clusters, of which we chose 6. After performing the k-means cluster analysis, we calculated the average probability for each ancestry for case individuals. Furthermore, we calculated the prevalence of MS in each cluster, and performed a one-sample t-test to investigate whether it differs from the overall MS prevalence (0.487%). This tests whether particular combinations of ancestry are associated with the phenotype at a SNP. Clusters with high MS risk-ratios have high Steppe components (Supplementary Figure 4.2), leading to the conclusion that Steppe ancestry alone is driving this signal.

WEIGHTED AVERAGE PREVALENCE

In order to quantify the risk of each ancestry for each SNP, we calculated the weighted average prevalence (WAP) for each ancestry based on the result of k-means clustering (above).

For the jth SNP, let $P_{jkm} = n_{jm}\underline{P}_{jkm}$ denote the sum of the kth ancestry probabilities of all the individuals in the mth cluster ($k, m = 1, \ldots, 6$), where n_{jm} is the cluster size of the mth cluster. Let π_{jm} denote the prevalence of MS in the mth cluster, the weighted average prevalence for the kth ancestry is defined as:

$$\underline{\pi}_{jk} = \frac{P_{jkm}\pi_{jm}}{\sum_{m=1}^{6} P_{jkm}},$$

where P_{jkm} is defined as the weight for each cluster.

For each ancestry, WAP measures the association of that ancestry with MS risk across all clusters. To make a clear comparison, we calculated the risk ratio (compared to the overall MS prevalence) for each ancestry at each SNP, and assigned a mean and confidence interval for the risk ratios of each ancestry at each chromosome (Figure3, Supplementary Figure 3.1 and 3.2).

PCA/UMAP OF WAP/AVERAGE DOSAGE

We performed principal component analysis (PCA) on the average ancestry probability and WAP at each MS-associated SNP (Supplementary Figure 4.3). The former shows that all of the HLA SNPs except three from HLA class II and III have much larger Outgroup components compared with the others. The latter analysis indicates a strong association between Steppe and MS risk. Also, Outgroup ancestry at rs10914539 from chromosome 1 exceptionally reduces the incidence of MS, while Outgroup ancestry at rs771767 (chromosome 3) and rs137956 (chromosome 22) significantly boosts MS risk.

ANCESTRAL RISK SCORES

Following methods developed in Irving-Pease et al. (*submitted*), we calculated the effect allele painting frequency for a given ancestry $f_{\{anc,i\}}$ for SNP i using the formula:

$$f_{\{anc,i\}} = \frac{\sum_{j}^{M_{effect}} \quad Painting\ certainty_{\{j,i,anc\}}}{\sum_{j}^{M_{alt}} \quad Painting\ certainty_{\{j,i,anc\}} + \sum_{j}^{M_{effect}} \quad Painting\ certainty_{\{j,i,anc\}}},$$

where there are M_{effect} individuals homozygous for the effect allele, M_{alt} individuals homozygous for the other allele, and $\sum_{j}^{M_{effect}} \quad Painting\ certainty_{\{j,i,anc\}}$ is the sum of the painting probabilities for that ancestry anc in individuals homozygous for the effect allele at SNP i. This can be interpreted as an estimate of an ancestral contribution to effect allele frequency in a modern population. Per-SNP painting frequencies can be found in ST4, ST5, and ST6.

To calculate the ancestral risk score (ARS) we summed over all I pruned SNPs in an additive model:

$$ARS_{anc} = \sum_{i}^{I} \quad f_{\{anc,i\}} * \ beta_i.$$

We then ran a transformation step as in [74]. To obtain 95% confidence intervals, we ran an accelerated bootstrap over loci, which accounts for the skew of data to better estimate confidence intervals [75].

LOCAL ANCESTRY AND GENOTYPE GWAS

We used the UK Biobank to fit GWAS models for local ancestry values and genotype values separately, using only SNPs known to be associated with the phenotype ('fine-mapped' SNPs). We

used the following phenotype codes for each phenotype: MS: Data-Field 131043; RA: Data-Field 131849 (seropositive); CD: Data-Field 21068.

Let Y_i denote the phenotype status for the ith individual ($i = 1,\ldots,399998$), which takes value 1 for a case and 0 for control, and let $\pi_i = Pr(Y_i = 1)$ denote the probability that this individual has the event. Let X_{ijk} denote the kth ancestry probability ($k = 1,\ldots,K$) for the jth SNP ($j = 1,\ldots,205$) of the ith individual. C_{ic} is the cth predictor ($c = 1,\ldots,N_c$) for the ith individual. We used the following logistic regression model for GWAS, which assumes the effects of alleles are additive:

$$Y_i \sim Bin(1,\pi_i);\ log(\frac{\pi_i}{1-\pi_i}) = \sum_{k=1}^{K} \beta_{jk} X_{ijk} + \sum_{c=1}^{N_c} \gamma_c\, C_{ic}.$$

We used N_c=20 predictors in the GWAS models, including sex, age and the first 18 PCs, which are sufficient to capture most of the population structure in the UK Biobank[76].

First, we built the model with $K = 1$. By using only one ancestry probability in each model, we aimed to find the statistical significance of each SNP under each ancestry. Then, we built the model with $K = 5$, i.e. using all 6 local ancestry probabilities which sum to 1. We calculated the variance explained by each SNP by summing up the variance explained by X_{ijk}(k=1,...,5).

We considered fitting the multivariate models by using all the SNPs as covariates. However, the dataset only contains 1,982 cases. Even though only one ancestry is included, the multivariate model contains 191 predictors, which could result in overfitting problems. Therefore, the GWAS models are preferred over multivariate models.

We also fitted a logistic regression model for GWAS using the genotype data as follows:

$$Y_i \sim Bin(1,\pi_i);\ log(\frac{\pi_i}{1-\pi_i}) = \beta_j X_{ij} + \sum_{c=1}^{N_c} \gamma_c\, C_{ic},$$

where $X_{ij} \in \{0,1,2\}$ denotes the number of copies of the reference allele of the jth SNP ($j = 1,\ldots,205$) that the ith individual has, and C_{ic} ($c = 1,\ldots,N_c$) denotes the covariates including age, sex and first 18 PCs for the ith individual, where N_c=20. Due to the UK Biobank being underpowered compared to the Case-Control study from which these SNPs were found, the only statistically significant (at $p < 10^{-5}$) association is in the HLA class II tagging HLA-DRB1*15:01.

COMPARISON OF GWAS MODELS USING PAINTING AND GENOTYPE DATA

We compared the variance explained by SNPs from the GWAS model using the painting data (all 6 local ancestry probabilities) with that from GWAS model using the genotype data. McFadden's pseudo R squared measure[77] is widely used for estimating the variance explained by the logistic regression models. McFadden's pseudo R squared is defined as

$$R^2 = 1 - \frac{ln(L_M)}{lm(L_0)},$$

where L_M and 0 are the likelihoods for the fitted and the null model, respectively. Taking overfitting into account, we propose the adjusted McFadden's pseudo R squared by penalizing the number of predictors:

$$Adjusted\ R^2 = 1 - \frac{ln(L_M)/(N-k)}{ln(L_0)/(N-1)},$$

where N is the sample size and k is the number of predictors.

Specifically, $R^2(SNPs)$ is calculated as the extra variance in addition to sex, age and 18 PCs that can be explained by SNPs:

$$R^2(SNPs) = R^2(sex + age + 18\,PCs + SNPs) - R^2(sex + age + 18\,PCs).$$

Notably, two SNPs stand out for explaining much larger variance than others when fitting the GWAS model using the genotype data, but overall more SNPs from GWAS painting explain more than 0.1% variance, which indicates the painting data are probably more efficient for estimating the effect sizes of SNPs and detecting significant SNPs. Also, some SNPs from GWAS models using painting data explain almost the same amount of variance, suggesting that these SNPs consist of very similar ancestries.

HAPLOTYPE TREND REGRESSION WITH eXtra FLEXIBILITY (HTRX)

We propose Haplotype Trend Regression with eXtra flexibility (HTRX) which searches for haplotype patterns that include single SNPs and non-contiguous haplotypes. HTRX is an association between a template of *n* SNPs and a phenotype. A template gives a value for each SNP taking values of '0' or '1', reflecting whether the reference allele of each SNP is present or absent, or an 'X' meaning either value is allowed. For example, haplotype '1X0' corresponds to a 3-SNP haplotype where the first SNP is the alternative allele and the third SNP is the reference allele, while the second SNP can be either the reference or the alternative allele. Therefore, haplotype '1X0' is essentially only a 2-SNP haplotype.

To examine the association between a haplotype and a binary phenotype, we replace the genotype term with a haplotype from the standard GWAS model:

$$Y_i \sim Bin(1, \pi_i);\ log(\frac{\pi_i}{1-\pi_i}) = \beta_j H_{ij} + \sum_{c=1}^{N_c} \gamma_c\, C_{ic},$$

where H_{ij} denotes the jth haplotype probability for the ith individual:

$$H_{ij} = \begin{cases} 1 & \text{if } i\text{th individual has haplotype } j \text{ in both genomes,} \\ 1/2 & \text{if } i\text{th individual has haplotype } j \text{ in one of the two genomes,} \\ 0 & \text{otherwise.} \end{cases}$$

HTRX can identify gene-gene interactions, and is superior to HTR not only because it can extract combinations of significant SNPs within a region, leading to improved predictive performance, but the haplotypes are more interpretable as multi-SNP haplotypes are only reported when they lead to increased predictive performance.

HTRX Model selection procedure for shorter haplotypes

Fitting HTRX models directly on the whole dataset can lead to significant overfitting, especially when the number of SNPs increases. When overfitting occurs, the models experience poorer predictive accuracy against unseen data. Further, HTRX introduces an enormous model space which much be searched.

To address these problems, we implement a two-step procedure.

Step 1: select **candidate** models. This is to address the model search problem, and is chosen to obtain a set of models more diverse than traditional bootstrap resampling (Efron, 1979[78]).

(1) Randomly sample a subset (50%) of data. Specifically, when the outcome is binary, stratified sampling is used to ensure the subset has approximately the same proportion of cases and controls as the whole data;

(2) Start from a model with fixed covariates (18 PCs, sex and age), and perform forward regression on the subset, i.e. iteratively choose a feature (in addition to the fixed covariates) to add whose inclusion enables the model to explain the largest variance, and select s models with the lowest Bayesian Information Criteria (BIC)[79] to enter the candidate model pool;

(3) repeat (1)-(2) B times, and select all the different models in the candidate model pool as the candidate models.

Step 2: select the best model using 10-fold cross-validation.

(1) Randomly split the whole data into 10 groups with approximately equal sizes, using stratified sampling when the outcome is binary;

(2) In each of the 10 folds, use a different group as the test dataset, and take the remaining groups as the training dataset. Then, fit all the candidate models on the training dataset, and use these fitted models to compute the additional variance explained by features (out-of-sample R^2) in the test dataset. Finally, select the candidate model with the biggest average out-of-sample R^2 as the best model.

HTRX Model selection procedure for longer haplotypes (Cumulative HTRX)

Longer haplotypes are important for discovering interactions. However, there are $3^k - 1$ haplotypes in HTRX if the region contains k SNPs, making it unrealistic for regions with large numbers of SNPs. To address this issue, we proposed cumulative HTRX to control the number of haplotypes, which is also a two-step procedure.

Step 1: extend haplotypes and select candidate models.

(1) Randomly sample a subset (50%) of data, use stratified sampling when the outcome is binary. This subset is used for all the analysis in (2) and (3);

(2) Start with L randomly chosen SNPs from the entire k SNPs, and keep the top M haplotypes that are chosen from the forward regression. Then add another SNP to the M haplotypes to create $3M + 2$ haplotypes. There are $3M$ haplotypes obtained by adding `0', `1' or `X' to the previous $M$ haplotypes, as well as 2 bases of the added SNP, i.e. `XX...X0' and `XX...X1' (as `X' was implicitly used in the previous step). The top M haplotypes from them are then selected using forward regression. Repeat this process until obtaining M haplotypes which include $k - 1$ SNPs;

(3) Add the last SNP to create $3M + 2$ haplotypes. Afterwards, start from a model with fixed covariates (18 PCs, sex and age), perform forward regression on the training set, and select s models with the lowest BIC to enter the candidate model pool;

(4) repeat (1)-(3) B times, and select all the different models in the candidate model pool as the candidate models.

Step 2: select the best model using 10-fold cross-validation, as described in "**HTRX Model selection procedure for shorter haplotypes**".

We note that because the search procedure in Step 1(2) may miss some highly predictive haplotypes, cumulative HTRX acts as a lower bound on the variance explainable by HTRX.

As a model criticism, only common and highly predictive haplotypes (i.e. those with the greatest adjusted R^2) are correctly identified, but the increased complexity of the search space of HTRX leads to haplotype subsets that are not significant on their own but are significant when interacting with other haplotype subsets being missed. This issue would be eased if we increase all the parameters s, l, M and B but with higher computational cost, or improve the search by optimizing the order of adding SNPs. This leads to a decreased certainty that the exact haplotypes proposed are `correct', but together reinforces the inference that interaction is extremely important.

Simulation for HTRX

To investigate how the total variance explained by HTRX compare to GWAS and HTR, we used a simulation study comparing:

(1) linear models (denoted by "lm") and generalized linear models with a logit link-function (denoted by "glm");

(2) models with or without actual interaction effects;

(3) models with or without rare SNPs (frequency smaller than 5%);

(4) remove or retain rare haplotypes when rare SNPs exist.

We started from creating the genotypes for 4 different SNPs G_{ijq} ($i = 1,\ldots,100{,}000$ denotes the index of individuals, $j = 1(\text{"}1XXX\text{"}), 2(\text{"}X1XX\text{"}), 3(\text{"}XX1X\text{"})\ and\ 4(\text{"}XXX1\text{"})$ represents the index of SNPs, and $q = 1{,}2$ for two genomes as individuals are diploid). If no rare SNPs were included, we sampled the frequency F_j of these 4 SNPs from 5% to 95%; otherwise, we sampled the frequency of the first 2 SNPs from 2% to 5% (in practice, we obtained $F_1 = 2.8\%$ and $F_2 = 3.1\%$ under our seed) while the last 2 SNPs from 5% to 95%. For the ith individual, we sampled $G_{ijq} \sim Bin(1, F_j)$ for the qth genome of the jth SNP, and took the average value of two genomes as the genotype for the jth SNP of the ith individual: $G_{ij} = \frac{G_{ij1}+G_{ij2}}{2}$. Based on the genotype data, we obtained the haplotype data for each individual, and we considered removing haplotypes rarer than 0.1% or not when rare SNPs were generated. In addition, we sampled 20 fixed covariates (including sex, age and 18 PCs) C_{ic} where $c = 1,\ldots,20$ from UK Biobank for 100000 individuals.

Next, we sampled the effect sizes of SNPs β_{G_j} and covariates β_{C_c}, and standardize them by their standard deviations: $\beta_{G_i} \sim \frac{U(-1,1)}{sd(G_j)}$ and $\beta_{C_c} \sim \frac{U(-1,1)}{sd(C_c)}$ for each fixed j and c, respectively. When interaction exists, we created a fixed effect size for haplotype "11XX" as twice the average absolute SNP effects: $\beta_{H_1} = \frac{1}{2}\sum_{j=1}^{4} |\beta_{G_j}|$ where H_1 refers to "11XX"; otherwise, $H_1 = 0$. Note that $F_{H_1} = 0.09\%$ when rare SNPs are included.

Finally, we sampled the outcome based on the outcome score (for the ith individual)

$$O_i = \sum_{c=1}^{20} \beta_c C_{ic} + \gamma(\sum_{j=1}^{4} \beta_{G_j} G_{ij} + \beta_{H_1} H_1) + e_i + w,$$

where γ is the effect scale of SNPs and haplotype "11XX", $e_i \sim N(0,0.1)$ is the random error and w is a fixed intercept term. For linear models, the outcome $Y_i = O_i$; while for generalized linear models, we sampled the outcome from binomial distribution: $Y_i \sim Bin(1, \pi_i)$, where $\pi_i = \frac{e^{O_i}}{1+e^{O_i}}$ is the probability that the i th individual has the case.

As the simulation is intended to compare the variance explained by HTRX, HTR and SNPs (GWAS) in addition to fixed covariates, we tripled the effect sizes of SNPs and haplotype "11XX" (if interaction exists) by setting $\gamma = 3$. In "glm", to ensure a reasonable case prevalence (e.g. below 5%), we set $w = -7$, which was also applied in "lm".

We applied the procedure described in " **HTRX Model selection procedure for shorter haplotypes**" for HTRX, HTR and GWAS, and visualized the distribution of the out-of-sample R^2 for each of the best models selected by each method in Supplementary Figure 4.4. In both "lm" and "glm", HTRX has equal predictive performance as the true model. It performs as well as GWAS when the interaction effects is absent, explains more variance when an interaction is present, and is significantly more explanatory than HTR. When rare SNPs are included, the only effective interaction term is rare. In this case the difference between GWAS and HTRX becomes smaller as expected, and removing the rare haplotypes hardly reduces the performance of HTRX.

In conclusion, we demonstrate through simulation that our HTRX implementation a) searches haplotype space effectively, and b) protects against overfitting. This makes it a superior approach compared to HTR and GWAS to integration SNP effects with gene-gene interaction. Its robustness also retains when there are rare effective SNPs and haplotypes.

POLYGENIC SELECTION TEST

We inferred allele frequency trajectories and selection coefficients for a set of LD-puned genome-wide significant trait associated variants using a modified version of the software CLUES[19]. To account for population structure in our samples, we applied a novel chromosome painting technique based on inference of a sample's nearest neighbours in the marginal trees of an ARG that contains labelled individuals (Irving-Pease et al., *submitted*). We ran CLUES using a time-series of imputed aDNA genotype probabilities obtained from 1,015 ancient West Eurasian samples that passed all quality control filters. We produced four additional models for each trait associated variant, by conditioning the analysis on one of the four ancestral path labels from our chromosome painting model: either Western hunter-gatherers (WHG), Eastern hunter-gatherers (EHG), Caucasus hunter-gatherers (CHG), or Anatolian farmers (ANA). We then inferred polygenic selection gradients (ω) and p-values for each of MS, CD and RA, in all ancestral paths, using the software PALM[20]. Full methods and results can be found in Supplementary Note 6.

ANCESTRY LINKAGE DISEQUILIBRIUM (LDA) AND ANCESTRY LINKAGE DISEQUILIBRIUM SCORE (LDAS)

In population genetics, linkage disequilibrium (LD) is defined as the non-random association of alleles at different loci in a given population[80]. We propose an ancestry linkage disequilibrium (LDA) approach to measure the association of ancestries between SNPs.

Let $A(i,j,k)$ denote the probability of the kth ancestry ($k = 1,\ldots,K$) at the jth SNP ($j = 1,\ldots,J$) of a chromosome for the ith individual ($i = 1,\ldots,N$).

We define the distance between SNP l and m as the average L_2 norm between ancestries at those SNPs. Specifically we compute the L_2 norm for the ith genome as

$$D_i(l,m) = ||A(i,l,\cdot) - A(i,m,\cdot)||_2 = \sqrt{\frac{1}{K}\sum_{k=1}^{K} \quad (A(i,l,k) - A(i,m,k))^2}.$$

Then we compute the distance between SNP l and m by averaging $D_i(l,m)$:

$$D(l,m) = \frac{1}{N}\sum_{i=1}^{N} \quad D_i(l,m).$$

We define $D^*(l,m)$ as the theoretical distance between SNP l and m if there were no linkage disequilibrium of ancestry (LDA) between them. $D^*(l,m)$ is estimated by

$$D^*(l,m) \approx \frac{1}{N}\sum_{i=1}^{N} \quad ||A(i^*,l,\cdot) - A(i,m,\cdot)||_2,$$

where $i^* \in \{1,\ldots,N\}$ are re-sampled without replacement at SNP l. Using the empirical distribution of ancestry probabilities accounts for variability in both the average ancestry and its distribution across SNPs. Ancestry assignment can be very precise in regions of the genome where our reference panel matches our data, and uncertain in others where we only have distant relatives of the underlying populations.

The LDA between SNP l and m is a similarity, defined in terms of the negative distance $-D(l,m)$ normalized by the expected value $D^*(l,m)$ under no LD, as:

$$LDA(l,m) = \frac{D^*(l,m) - D(l,m)}{D^*(l,m)}.$$

LDA therefore takes an expected value 0 when haplotypes are randomly assigned at different SNPs, and positive values when the ancestries of haplotypes are correlated.

LDA is a pairwise quantity. To arrive at a per-SNP property, we define the LDA score (LDAS) of SNP j as the total LDA of this SNP with the rest of the genome, i.e. the integral of the LDA for that SNP. Because this quantity decreases to zero as we move away from the target SNP, this is in practice computed within an XcM-window (we use $X = 5$ as LDA is approximately zero outside this region in our data) on both sides of the SNP. Note that we measure this quantity in terms of the genetic distance, and therefore LDAS is measuring the length of ancestry-specific haplotypes compared to individual-level recombination rates.

As a technical note, when the SNPs approach either end of the chromosome, they no longer have a complete window, which results in a smaller LDAS. This would be appropriate for measuring total ancestry correlations, but to make LDAS useful for detecting anomalous SNPs, we use the LDAS of the symmetric side of the SNP to estimate the LDAS within the non-existent window.

$$LDAS(j;X) = \begin{cases} \int_{gd(j)-X}^{gd(j)+X} LDA(j,l)\,dgd & \text{if } X \le gd(j) \le tg - X, \\ \int_{0}^{gd(j)+X} LDA(j,l)\,dgd + \int_{2gd(j)}^{gd(j)+X} LDA(j,l)\,dgd & \text{if } gd(j) < X, \\ \int_{gd(j)-X}^{tg} LDA(j,l)\,dgd + \int_{gd(j)-X}^{2gd(j)-tg} LDA(j,l)\,dgd & \text{if } gd(j) > tg - X. \end{cases}$$

where $gd(l)$ is the genetic distance (i.e. position in cM) of SNP l, and tg is the total genetic distance of a chromosome. We also assume the LDA on either end of the chromosome equals the LDA of the SNP closest to the end: $LDA(j, gd = 0) = LDA(j, l_{min(gd)})$ and $LDA(j, gd = td) = LDA(j, l_{max(gd)})$, where gd is the genetic distance, $l_{min(gd)}$ and $l_{max(gd)}$ are the indexes of the SNP with the smallest and largest genetic distance, respectively.

The integral $\int_{gd(j)-X}^{gd(j)+X} LDA(j, l) dgd$ is computed assuming linear interpolation of the LDA score between adjacent SNPs.

LDA thus quantifies the correlations between the ancestry of two SNPs, measuring the proportion of individuals who have experienced a recombination leading to a change in ancestry, relative to the genome-wide baseline. The LDA score is the total amount of genome in LDA with each SNP (measured in recombination map distance).

SIMULATION FOR SELECTION: LDA

An ancient population P_0 evolved for 2200 generations before splitting into two sub-populations P_1 (Steppe) and P_2 (Farmer). After evolving 400 generations, we added mutation "m_1" and "m_2" at the different locus in P_1 and P_2. Both added mutations were then positively selected in the following 300 generations, after which they merged to P_3, where both added mutations experienced strong positive selection for 20 generations. Finally, we sampled 1000 individuals from P_3 to compute their ancestry proportions of P_1 and P_2 using the "chromosome painting" technique, and calculated the LDA score of the simulated chromosome positions.

The above describes the simulation in Supplementary Figure 6.1.

We investigated balancing selection at 2 loci as well. The balancing selection in P_1 and P_2 ensured the mutated allele reaches around 50% frequency, while positive selection made the mutated allele become almost the only allele. In P_3, if m_1 or m_2 was positively selected, its frequency reached more than 80% regardless of whether the allele experienced balancing or positive selection in P_1 or P_2, because we set a strong positive selection. If m_1 or m_2 was balancing selected in P_3, its frequency slightly increased, e.g. if m_1 underwent balancing selection in P_1, it had 25% frequency when P_3 was created, and the frequency reached around 37.5% after 20 generations of balancing selection in P_3.

The results (Supplementary Figure 6.2) show that positive selection in P_3 resulted in low LDA scores around the selected locus, if this allele was not uncommon (i.e. had 50% (balancing selection) or 100% frequency (positive selection) in subpopulation P_1 or P_2). Note that the balancing selection in P_1 or P_2 worked the same as "weak positive selection", because m_1 and m_2 were rare when they first occurred, which were positively selected until 50% frequency.

We also performed simulations for selection at a single locus (Supplementary Figure 6.2&6.3).

Stage 1: We added a mutation m_1 in the 1600 generation in P_0, which then underwent balancing selection until generation 2200, when P_0 split into P_1 and P_2, where the frequency of m_1 was around 50%.

Stage 2: Then we explored different combinations of positive, balancing and negative selection of m_1 in P_1 and P_2. the frequency of m_1 reached 80%, 50% and 20% when it was positively, balancing or negatively selected, respectively, until generation 2899. Here we sampled 20 individuals each in P_1 and P_2 as the ancient samples.

Stage 3: Then P_1 and P_2 merged into P_3 in generation 2900. In P_3, for each combination of selection in Stage 2, we simulated positive, balancing and negative selection for m_1. The selection lasted for 20 generations, and then we sampled 4000 individuals from P_3 as the modern population.

Results: when m_1 was positively selected in only one of P_1 and P_2, and it experienced negative selection in P_3, the LDA scores around the locus of m_1 were low. Otherwise, no abnormal LDA scores were found at m_1.

REFERENCES

1. Walton, C. *et al.* Rising prevalence of multiple sclerosis worldwide: Insights from the Atlas of MS, third edition. *Mult. Scler. J.* **26**, 1816–1821 (2020).
2. Attfield, K. E., Jensen, L. T., Kaufmann, M., Friese, M. A. & Fugger, L. The immunology of multiple sclerosis. *Nat. Rev. Immunol.* (2022) doi:10.1038/s41577-022-00718-z.
3. International Multiple Sclerosis Genetics Consortium *et al.* Multiple sclerosis genomic map implicates peripheral immune cells and microglia in susceptibility. *Science* **365**, eaav7188 (2019).
4. Bjornevik, K. *et al.* Longitudinal analysis reveals high prevalence of Epstein-Barr virus associated with multiple sclerosis. *Science* **375**, 296–301 (2022).
5. Lanz, T. V. *et al.* Clonally expanded B cells in multiple sclerosis bind EBV EBNA1 and GlialCAM. *Nature* **603**, 321–327 (2022).
6. Olsson, T., Barcellos, L. F. & Alfredsson, L. Interactions between genetic, lifestyle and environmental risk factors for multiple sclerosis. *Nat. Rev. Neurol.* **13**, 25–36 (2017).
7. Benton, M. L. *et al.* The influence of evolutionary history on human health and disease. *Nat. Rev. Genet.* **22**, 269–283 (2021).
8. Chi, C. *et al.* Admixture mapping reveals evidence of differential multiple sclerosis risk by genetic ancestry. *PLOS Genet.* **15**, e1007808 (2019).
9. Allentoft, M. E. *et al. Population Genomics of Stone Age Eurasia*. http://biorxiv.org/lookup/doi/10.1101/2022.05.04.490594 (2022) doi:10.1101/2022.05.04.490594.
10. Haak, W. *et al.* Massive migration from the steppe was a source for Indo-European languages in Europe. *Nature* **522**, 207–211 (2015).
11. Jones, E. R. *et al.* Upper Palaeolithic genomes reveal deep roots of modern Eurasians. *Nat. Commun.* **6**, 8912 (2015).
12. Allentoft, M. E. *et al.* Population genomics of Bronze Age Eurasia. *Nature* **522**, 167–172 (2015).
13. Bycroft, C. *et al.* The UK Biobank resource with deep phenotyping and genomic data. *Nature* **562**, 203–209 (2018).
14. Itan, Y., Powell, A., Beaumont, M. A., Burger, J. & Thomas, M. G. The Origins of Lactase

Persistence in Europe. *PLoS Comput. Biol.* **5**, e1000491 (2009).

15. Dehasque, M. *et al.* Inference of natural selection from ancient DNA. *Evol. Lett.* **4**, 94–108 (2020).

16. Efron, B. Better Bootstrap Confidence Intervals. *J. Am. Stat. Assoc.* **82**, 171–185 (1987).

17. Zaykin, D. V. *et al.* Testing Association of Statistically Inferred Haplotypes with Discrete and Continuous Traits in Samples of Unrelated Individuals. *Hum. Hered.* **53**, 79–91 (2002).

18. Thuesen, N. H., Klausen, M. S., Gopalakrishnan, S., Trolle, T. & Renaud, G. *Benchmarking freely available human leukocyte antigen typing algorithms across varying genes, coverages and typing resolutions*. http://biorxiv.org/lookup/doi/10.1101/2022.06.28.497888 (2022) doi:10.1101/2022.06.28.497888.

19. Stern, A. J., Wilton, P. R. & Nielsen, R. An approximate full-likelihood method for inferring selection and allele frequency trajectories from DNA sequence data. *PLOS Genet.* **15**, e1008384 (2019).

20. Stern, A. J., Speidel, L., Zaitlen, N. A. & Nielsen, R. Disentangling selection on genetically correlated polygenic traits via whole-genome genealogies. *Am. J. Hum. Genet.* **108**, 219–239 (2021).

21. Comabella, M. *et al.* Identification of a Novel Risk Locus for Multiple Sclerosis at 13q31.3 by a Pooled Genome-Wide Scan of 500,000 Single Nucleotide Polymorphisms. *PLoS ONE* **3**, e3490 (2008).

22. Bersaglieri, T. *et al.* Genetic Signatures of Strong Recent Positive Selection at the Lactase Gene. *Am. J. Hum. Genet.* **74**, 1111–1120 (2004).

23. He, Z., Dai, X., Beaumont, M. & Yu, F. Detecting and Quantifying Natural Selection at Two Linked Loci from Time Series Data of Allele Frequencies with Forward-in-Time Simulations. *Genetics* **216**, 521–541 (2020).

24. Fugger, L., Jensen, L. T. & Rossjohn, J. Challenges, Progress, and Prospects of Developing Therapies to Treat Autoimmune Diseases. *Cell* **181**, 63–80 (2020).

25. Gregersen, J. W. *et al.* Functional epistasis on a common MHC haplotype associated with multiple sclerosis. *Nature* **443**, 574–577 (2006).

26. Wang, J. H. *et al.* Modeling the cumulative genetic risk for multiple sclerosis from genome-wide association data. *Genome Med.* **3**, 3 (2011).

27. Cotsapas, C. & Mitrovic, M. Genome-wide association studies of multiple sclerosis. *Clin. Transl. Immunol.* **7**, e1018 (2018).

28. Slim, L., Chatelain, C., Foucauld, H. de & Azencott, C.-A. A systematic analysis of gene–gene interaction in multiple sclerosis. *BMC Med. Genomics* **15**, 100 (2022).

29. Bos, K. I. *et al.* Pre-Columbian mycobacterial genomes reveal seals as a source of New World human tuberculosis. *Nature* **514**, 494–497 (2014).

30. Sabin, S. *et al.* A seventeenth-century Mycobacterium tuberculosis genome supports a Neolithic emergence of the Mycobacterium tuberculosis complex. *Genome Biol.* **21**, 201 (2020).

31. Rasmussen, S. *et al.* Early Divergent Strains of Yersinia pestis in Eurasia 5,000 Years Ago. *Cell* **163**, 571–582 (2015).

32. Spyrou, M. A. *et al.* Analysis of 3800-year-old Yersinia pestis genomes suggests Bronze Age origin for bubonic plague. *Nat. Commun.* **9**, 2234 (2018).

33. Rascovan, N. *et al.* Emergence and Spread of Basal Lineages of Yersinia pestis during the Neolithic Decline. *Cell* **176**, 295-305.e10 (2019).

34. Guellil, M. *et al.* Ancient herpes simplex 1 genomes reveal recent viral structure in Eurasia. *Sci. Adv.* **8**, eabo4435.

35. Pontremoli, C., Forni, D., Clerici, M., Cagliani, R. & Sironi, M. Possible European Origin of Circulating Varicella Zoster Virus Strains. *J. Infect. Dis.* jiz227 (2019) doi:10.1093/infdis/jiz227.

36. Tian, C. *et al.* Genome-wide association and HLA region fine-mapping studies identify susceptibility loci for multiple common infections. *Nat. Commun.* **8**, 599 (2017).

37. Krause-Kyora, B. *et al.* Ancient DNA study reveals HLA susceptibility locus for leprosy in medieval Europeans. *Nat. Commun.* **9**, 1569 (2018).

38. Wallin, M. T. *et al.* The prevalence of MS in the United States: A population-based estimate using health claims data. *Neurology* **92**, e1029–e1040 (2019).

39. Feigin, V. L. *et al.* Global, regional, and national burden of neurological disorders, 1990–2016: a systematic analysis for the Global Burden of Disease Study 2016. *Lancet Neurol.* **18**, 459–

480 (2019).

40. Fleming, J. & Fabry, Z. The hygiene hypothesis and multiple sclerosis. *Ann. Neurol.* **61**, 85–89 (2007).

41. Joo, Y. B., Lim, Y.-H., Kim, K.-J., Park, K.-S. & Park, Y.-J. Respiratory viral infections and the risk of rheumatoid arthritis. *Arthritis Res. Ther.* **21**, 199 (2019).

42. Safiri, S. *et al.* Global, regional and national burden of rheumatoid arthritis 1990–2017: a systematic analysis of the Global Burden of Disease study 2017. *Ann. Rheum. Dis.* **78**, 1463–1471 (2019).

43. Lindfors, K. *et al.* Coeliac disease. *Nat. Rev. Dis. Primer* **5**, 3 (2019).

44. Rubinacci, S., Ribeiro, D. M., Hofmeister, R. J. & Delaneau, O. Efficient phasing and imputation of low-coverage sequencing data using large reference panels. *Nat. Genet.* **53**, 120–126 (2021).

45. Meyer, M. & Kircher, M. Illumina Sequencing Library Preparation for Highly Multiplexed Target Capture and Sequencing. *Cold Spring Harb. Protoc.* **2010**, pdb.prot5448 (2010).

46. Schubert, M., Lindgreen, S. & Orlando, L. AdapterRemoval v2: rapid adapter trimming, identification, and read merging. *BMC Res. Notes* **9**, 88 (2016).

47. Li, H. & Durbin, R. Fast and accurate short read alignment with Burrows-Wheeler transform. *Bioinformatics* **25**, 1754–1760 (2009).

48. Li, H. *et al.* The Sequence Alignment/Map format and SAMtools. *Bioinformatics* **25**, 2078–2079 (2009).

49. Jónsson, H., Ginolhac, A., Schubert, M., Johnson, P. L. F. & Orlando, L. mapDamage2.0: fast approximate Bayesian estimates of ancient DNA damage parameters. *Bioinformatics* **29**, 1682–1684 (2013).

50. Fu, Q. *et al.* A Revised Timescale for Human Evolution Based on Ancient Mitochondrial Genomes. *Curr. Biol.* **23**, 553–559 (2013).

51. Korneliussen, T. S., Albrechtsen, A. & Nielsen, R. ANGSD: Analysis of Next Generation Sequencing Data. *BMC Bioinformatics* **15**, 356 (2014).

52. Monroy Kuhn, J. M., Jakobsson, M. & Günther, T. Estimating genetic kin relationships in

prehistoric populations. *PLOS ONE* **13**, e0195491 (2018).

53. Weissensteiner, H. *et al.* HaploGrep 2: mitochondrial haplogroup classification in the era of high-throughput sequencing. *Nucleic Acids Res.* **44**, W58–W63 (2016).

54. Scorrano, G., Yediay, F. E., Pinotti, T., Feizabadifarahani, M. & Kristiansen, K. The genetic and cultural impact of the Steppe migration into Europe. *Ann. Hum. Biol.* **48**, 223–233 (2021).

55. Purcell, S. *et al.* PLINK: A Tool Set for Whole-Genome Association and Population-Based Linkage Analyses. *Am. J. Hum. Genet.* **81**, 559–575 (2007).

56. Shringarpure, S. S., Bustamante, C. D., Lange, K. & Alexander, D. H. Efficient analysis of large datasets and sex bias with ADMIXTURE. *BMC Bioinformatics* **17**, 218 (2016).

57. Patterson, N. *et al.* Ancient Admixture in Human History. *Genetics* **192**, 1065–1093 (2012).

58. Lawson, D. J., Hellenthal, G., Myers, S. & Falush, D. Inference of Population Structure using Dense Haplotype Data. *PLoS Genet.* **8**, e1002453 (2012).

59. Margaryan, A. *et al.* Population genomics of the Viking world. *Nature* **585**, 390–396 (2020).

60. Hellenthal, G. *et al.* A Genetic Atlas of Human Admixture History. *Science* **343**, 747–751 (2014).

61. The 1000 Genomes Project Consortium *et al.* A global reference for human genetic variation. *Nature* **526**, 68–74 (2015).

62. Myers, T. A., Chanock, S. J. & Machiela, M. J. LDlinkR: An R Package for Rapidly Calculating Linkage Disequilibrium Statistics in Diverse Populations. *Front. Genet.* **11**, 157 (2020).

63. Ishigaki, K. *et al. Trans-ancestry genome-wide association study identifies novel genetic mechanisms in rheumatoid arthritis*. http://medrxiv.org/lookup/doi/10.1101/2021.12.01.21267132 (2021) doi:10.1101/2021.12.01.21267132.

64. Alekseyenko, A. V. *et al.* Causal graph-based analysis of genome-wide association data in rheumatoid arthritis. *Biol. Direct* **6**, 25 (2011).

65. Raychaudhuri, S. *et al.* Five amino acids in three HLA proteins explain most of the association between MHC and seropositive rheumatoid arthritis. *Nat. Genet.* **44**, 291–296 (2012).

66. Spanish Consortium on the Genetics of Coeliac Disease (CEGEC) *et al.* Dense genotyping

identifies and localizes multiple common and rare variant association signals in celiac disease. *Nat. Genet.* **43**, 1193–1201 (2011).

67. Monsuur, A. J. *et al.* Effective Detection of Human Leukocyte Antigen Risk Alleles in Celiac Disease Using Tag Single Nucleotide Polymorphisms. *PLoS ONE* **3**, e2270 (2008).

68. Gutierrez-Achury, J. *et al.* Fine mapping in the MHC region accounts for 18% additional genetic risk for celiac disease. *Nat. Genet.* **47**, 577–578 (2015).

69. the RACI consortium *et al.* Genetics of rheumatoid arthritis contributes to biology and drug discovery. *Nature* **506**, 376–381 (2014).

70. Chang, C. C. *et al.* Second-generation PLINK: rising to the challenge of larger and richer datasets. *GigaScience* **4**, 7 (2015).

71. Ju, D. & Mathieson, I. The evolution of skin pigmentation-associated variation in West Eurasia. *Proc. Natl. Acad. Sci.* **118**, e2009227118 (2021).

72. Kolberg, L., Raudvere, U., Kuzmin, I., Vilo, J. & Peterson, H. gprofiler2 -- an R package for gene list functional enrichment analysis and namespace conversion toolset g:Profiler. *F1000Research* **9**, ELIXIR-709 (2020).

73. Thorndike, R. L. Who belongs in the family? *Psychometrika* **18**, 267–276 (1953).

74. Berg, J. J. & Coop, G. A Population Genetic Signal of Polygenic Adaptation. *PLoS Genet.* **10**, e1004412 (2014).

75. Frangos, C. C. & Schucany, W. R. Jackknife estimation of the bootstrap acceleration constant. *Comput. Stat. Data Anal.* **9**, 271–281 (1990).

76. Sarmanova, A., Morris, T. & Lawson, D. J. *Population stratification in GWAS meta-analysis should be standardized to the best available reference datasets*. http://biorxiv.org/lookup/doi/10.1101/2020.09.03.281568 (2020) doi:10.1101/2020.09.03.281568.

77. McFadden, D. Conditional logit analysis of qualitative choice behavior. (1973).

78. Efron, B. Bootstrap Methods: Another Look at the Jackknife. *Ann. Stat.* **7**, 1–26 (1979).

79. Kass, R. E. & Wasserman, L. A Reference Bayesian Test for Nested Hypotheses and its Relationship to the Schwarz Criterion. *J. Am. Stat. Assoc.* **90**, 928–934 (1995).

80. Slatkin, M. Linkage disequilibrium — understanding the evolutionary past and mapping the

medical future. *Nat. Rev. Genet.* **9**, 477–485 (2008).